

PREDICTION OF COUPLING GUARD TEMPERATURE
AND GEARBOX WINDAGE POWER LOSS

A Thesis

by

TIANBO ZHAI

Submitted to the Office of Graduate and Professional Studies of
Texas A&M University
in partial fulfillment of the requirements for the degree of

MASTER OF SCIENCE

Chair of Committee,	Alan Palazzolo
Committee Members,	Je-Chin Han
	Hamn-Ching Chen
Head of Department,	Andreas A. Polycarpou

December 2016

Major Subject: Mechanical Engineering

Copyright 2016 Tianbo Zhai

ABSTRACT

Gear Windage Power Loss (WPL) is due to fluid drag experienced by a gear when it is rotating in air or an air-oil mist. Gear WPL becomes significant and shall not be neglected in high speed applications. The temperature on coupling guard needs to comply with industry standards and is influenced by windage affect. There is practical significance in predicting coupling guard temperature and gearbox WPL.

Simulation models were built and results were obtained from Computational Fluid Dynamics (CFD) solvers. The simulation results were validated by experimental data from the literature. A case study was also conducted to further validate the predictability of coupling guard temperature. Simulation experiments were designed and data generated to obtain Multivariable Regression Formulas (MRF) for gear WPL and guard temperature prediction.

A comparison between CFD prediction of gear WPL and experimental results showed a relative error less than 12%. In the case study, the percentage difference between predicted guard temperature and test data was within 5%. For the given ranges of input parameters, MRF gave a better prediction than the empirical formula used in industry.

The proposed MRF was accurate for coupling guards and gears that were not included in the CFD modeled systems, which were used to generate the data for obtaining the MRF. The prediction expressions also helped in the product design stage to mitigate gearbox WPL and coupling guard temperature.

To Yashu, my love

ACKNOWLEDGEMENTS

I would like to thank my committee chair, Dr. Palazzolo, who provided me the opportunity to conduct the research project and supported me throughout my master's studies. Thanks also goes to my committee members, Dr. Han and Dr. Chen, for their guidance during the research.

I would like to thank Greg Elliott and Chad Robertson (GE Oil and Gas) for initiating the research topics and discussing ideas with me. Thank you, James Hardin (Elliott Group), Yves Bidaut (MAN Diesel & Turbo), Patrick Potter (Cincinnati Gearing System) and Bryan Lobo (ANSYS) for sharing their industrial insights. Thank you, Yann Marchesse, for answering my questions regarding this paper. Thank you, Dr. Hartwig, for his advice about writing a scientific paper. Thank you, High Performance Research Computing, for its supercomputing facilities and the technical support provided. Special thanks go to Adam Thompson and Steve Pennington (John Crane), who shared experimental data from their test rig in support of the research and made my internship in England a unique experience.

Thanks also goes to my lab members and the faculty and staff at Texas A&M who have always been helpful. I want to extend my gratitude to the Turbomachinery Research Consortium (TRC), which provided the funding to this study.

Finally, thank you, my parents and family members, for their kindly encouragement and love.

CONTRIBUTORS AND FUNDING SOURCES

Contributors

This work was supervised by a thesis committee consisting of Professor Alan Palazzolo and Je-Chin Han of the Department of Mechanical Engineering and Professor Hamn-Ching Chen of the Department of Civil Engineering.

The data analyzed for Section 3 was provided by Mr. Adam Thompson from John Crane. The analyses depicted in Section 3 were conducted in part by Mr. Adam Thompson and were published in 2016.

All other work conducted for the thesis was completed by the student independently.

Funding Sources

This work was made possible in part by Turbomachinery Research Consortium (TRC) under Project Number 400124 - 00043.

NOMENCLATURE

A	Arrangement constant
b	Total face width
d'	Operating pitch diameter of gear
D	Characteristic diameter
D_c	Diameter of the coupling guard
\bar{h}	Heat transfer coefficient
g	Acceleration due to gravity
L	Length of rotating element
m_n	Normal module
n	Gear speed
P_w	Power loss due to windage, total
P_m	Power loss due to windage, modified
P_{w_side}	Power loss due to windage, from gear side
$P_{w_periphery}$	Power loss due to windage, from gear periphery
P_w'	Windage power loss per gear
Ra_D	Rayleigh number
R_f	Rough surface adjustment factor, related to diametral pitch
Re	Reynolds number

T_a	Ambient temperature
T_c	Coupling temperature
T_e	Enclosure temperature
T_s	Surface temperature
T_{ave}	Volume average temperature of coupling guard
T_{shaft}	Shaft temperature
V	Maximum velocity of the coupling relative to the fluid
ν	Kinematic viscosity
β	Thermal expansion coefficient
β'	Operating helix angle
Ψ	Helix angle

TABLE OF CONTENTS

	Page
ABSTRACT	ii
DEDICATION	iii
ACKNOWLEDGEMENTS	iv
CONTRIBUTORS AND FUNDING SOURCES.....	v
NOMENCLATURE.....	vi
TABLE OF CONTENTS	viii
LIST OF FIGURES.....	x
LIST OF TABLES	xiv
1 INTRODUCTION.....	1
1.1 Background	1
1.2 Literature review	4
1.3 Research objectives	11
2 COUPLING GUARD TEMPERATURE AND WINDAGE POWER LOSS: A CASE STUDY	12
2.1 Problem description.....	12
2.2 Physical testing.....	13
2.3 Steady state simulation in ANSYS CFX.....	16
2.4 Lessons learned	28
3 REGRESSION MODEL FOR COUPLING GUARD TEMPERATURE PREDICTION	30
3.1 Calistrat’s empirical formula for temperature prediction.....	30
3.2 Multivariable regression formulas for temperature prediction	32
3.3 Validation and comparison with empirical model	51
4 REGRESSION MODEL FOR GEAR WINDAGE POWER LOSS.....	55

4.1	Empirical formula for gear WPL calculation	55
4.2	Gear WPL calculation using CFD methods	59
4.3	Gear windage power loss regression model	75
4.4	Two meshing spur gears simulation in Fluent (3D, transient)	82
5	CONCLUSION AND FUTURE WORK	91
5.1	Conclusion	91
5.2	Future work	92
	REFERENCES	93
	APPENDIX A TUTORIAL FOR TWO MESHING GEAR SIMULATION IN FLUENT	97
	APPENDIX B TUTORIAL FOR COUPLING GUARD TEMPERATURE SIMULATION IN CFX	108
	APPENDIX C DESIGN OF EXPERIMENTS IN JMP	114

LIST OF FIGURES

	Page
Figure 1.1 Flow Pattern in Gear Teeth Region	2
Figure 1.2 High Performance Disc Coupling.....	2
Figure 1.3 Coupling and Coupling Guard.....	3
Figure 1.4 Coupling and Coupling Enclosure/Guard.....	4
Figure 1.5 Temperature Prediction by Revised Formula (Wind) and Comparison	5
Figure 1.6 Section View of Coupling with Windage Flange	6
Figure 1.7 Coupling Guard on a Turbo Expander.....	6
Figure 1.8 Mesh for Gear Teeth with 5mm Peripheral Shroud.....	7
Figure 1.9 Experimental and Numerical Windage Power Loss	8
Figure 1.10 Numerical Domain and Boundary Conditions for Helical Gear WPL Simulation.....	9
Figure 1.11 Velocity Streamline of Two Meshing Gear	10
Figure 1.12 Velocity Contour of the Lubricant Within Gearbox	10
Figure 2.1 Test Rig Overview	14
Figure 2.2 Location of Thermocouples (TC1 to TC6) and Pressure Transducers (P1 to P4).....	15
Figure 2.3 A 1/4 Section of Computational Domain	16
Figure 2.4 Cross Section of Mesh Showing Four Domains	17
Figure 2.5 Radial Clearances of Coupling Guard	18
Figure 2.6 Boundary Conditions of CFD Model.....	20
Figure 2.7 Temperature Contour Plot with 2D Streamline Overlay for Configuration 4: Medium Size Guard Without Windage Flanges.....	22

	Page
Figure 2.8 Coupling Temperature Contour Plot for Configuration 4: Medium Size Guard Without Windage Flanges	23
Figure 2.9 Comparison Between Simulation Results and Physical Test Results for Test Configuration 4: Medium Guard Without Windage Flanges	24
Figure 3.1 Input Parameters in Calistrat’s Empirical Formula	30
Figure 3.2 Coupling Geometry and Cross Section View with Coupling Guard	32
Figure 3.3 Key Dimensions of Computational Domain.....	33
Figure 3.4 Parameters in Regression Based Model.....	35
Figure 3.5 Computational Domain.....	38
Figure 3.6 Mesh for 1/4 of the Computational Domain.....	40
Figure 3.7 Periodic Boundary Conditions.....	40
Figure 3.8 Temperature Contour of Coupling Guard.....	45
Figure 3.9 Temperature Contour within Coupling Enclosure and on Coupling	46
Figure 3.10 Negative Pressure Region Within Coupling Enclosure	47
Figure 3.11 Relationship Between Reference Value and Value Calculated by Calistrat’s Formula	52
Figure 3.12 Relationship Between Reference Value and Value Calculated by Regression-based Formula.....	53
Figure 4.1 Boundary Conditions in Fluent.....	61
Figure 4.2 Pressure Contour and Velocity Streamline for 2D Spur Gear	62
Figure 4.3 Simulation Results Summary.....	63
Figure 4.4 Experimental Data from Lord’s Paper.....	64
Figure 4.5 WPL vs. Non-dimensional Shroud Clearance	65
Figure 4.6 WPL vs. Peripheral Clearance	66

	Page
Figure 4.7 Structured Mesh for Two Spur Gear Teeth	67
Figure 4.8 Pressure Contour of Gear Teeth @ 400 rad/s	69
Figure 4.9 Velocity Streamline @ 400 rad/s.....	70
Figure 4.10 Comparison of CFD and Experiment Results for 3D Spur Gear Model	71
Figure 4.11 Simulation Domain Derived From Whole Gear	72
Figure 4.12 Structured Mesh of Helical Gear Teeth	72
Figure 4.13 Pressure Contour of Helical Gear Teeth @ 200 rad/s.....	73
Figure 4.14 Velocity Streamline of Helical Gear @ 200rad/s	73
Figure 4.15 Helical Gear WPL Comparison	74
Figure 4.16 Relationship Between Reference Value and Value Calculated by Regression-based Formula.....	79
Figure 4.17 Relationship Between Reference Value and Value Calculated by Empirical Formula	80
Figure 4.18 Comparison Between Regression and Experimental Results	81
Figure 4.19 Test Cases Points Plotted in Red	82
Figure 4.20 Numerical Model of Gearbox	84
Figure 4.21 Velocity Contour at 0.01s of Flow Time	85
Figure 4.22 Velocity Contour at 0.025s of Flow Time	85
Figure 4.23 Pressure Contour at 0.01s of Flow Time	85
Figure 4.24 Pressure Contour at 0.025s of Flow Time	85
Figure 4.25 Evolution of Torque on Gear Teeth 1 & 2 @2000rpm.....	86
Figure 4.26 Evolution of Power Loss on Gear Teeth 1 & 2 @2000rpm	87
Figure 4.27 Evolution of Torque on Gear Teeth 1 & 2 @5000rpm.....	88
Figure 4.28 Evolution of Torque on Gear Teeth 1 & 2 @6000rpm.....	88

	Page
PageFigure 4.29 Experimental Results from Literature for Comparison.....	90

LIST OF TABLES

	Page
Table 2.1 Physical Test Configurations	13
Table 2.2 Comparison Between Test and Simulation for Test Configuration 4	23
Table 2.3 Contours in CFD-POST and Analysis	25
Table 3.1 Input Parameters for Initial Simulation.....	33
Table 3.2 Mesh Independence Study	39
Table 3.3 Boundary Conditions in CFX.....	41
Table 3.4 Proposed Correlation for Natural Convection from Horizontal Cylinders	43
Table 3.5 Output Parameters for Sample Simulation.....	45
Table 3.6 Design of Simulation Experiments and Results Reported in ANSYS CFX	49
Table 3.7 Input and Output of Test Case T1	51
Table 3.8 Parameter Ranges.....	54
Table 4.1 Relationship Between m_t and R_f	58
Table 4.2 Helical Gear Geometry	58
Table 4.3 Spur Gear Geometry for 2D Simulation	61
Table 4.4 Spur Gear Geometry for 3D Simulation	66
Table 4.5 Boundary Conditions for 3D Gear Simulation.....	68
Table 4.6 Parameters and Their Ranges.....	75
Table 4.7 Design of Experiments and Simulation Results.....	76
Table 4.8 Gear Geometry for Test Case.....	80
Table 4.9 Parameters in Test Cases.....	81

	Page
Table 4.10 Gear Geometry for Meshing Gear Simulation	83

1 INTRODUCTION

1.1 Background

For gearboxes, there are many different types of power loss; meshing losses, bearing losses, windage losses, etc. For a high rate gearbox which exceed 100 MW [1], 1% loss in efficiency equals as much as 1 MW loss in energy. To mitigate these losses and increase efficiency of a gearbox is important.

Gear Windage Power Loss (WPL) is due to the fluid drag experienced by the gear when it is running in air or an air-oil mist [2]. When pitch line velocity is above 10,000 ft/min (50.8m/s), gear WPL becomes significant and shall not be ignored [3]. Both experimental and simulation results exist in open literature for the WPL generated by an individual spur or helical gear rotating in air.

With recent advancement of Computational Fluid Dynamic (CFD), WPL can be estimated computationally and multiple factors that affect WPL can be identified. Figure 1.1 shows the flow pattern when a spur gear rotating in air at 700 rad/s. The windage torque on the gear teeth can be obtained from post-processing. Gear WPL is then calculated from multiplying the torque by rotating speed.

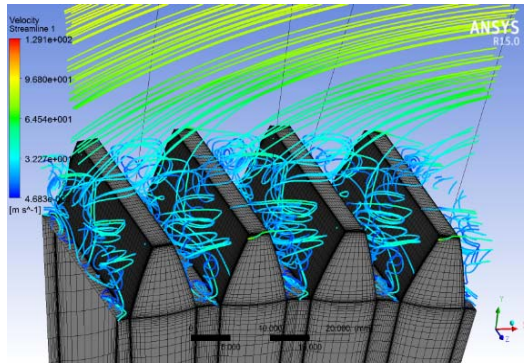


Figure 1.1 Flow Pattern in Gear Teeth Region

A Coupling is a mechanical device used to transmit power (Torque and speed) between the rotating shafts of driver and driven machines, it also allows for some misalignment between the shafts. Figure 1.2 shows a disc coupling for high speed applications. The torque is transmitted between the bolts through a series of thin disc assembled in a pack. The hub of the coupling is also indicated in below figure.

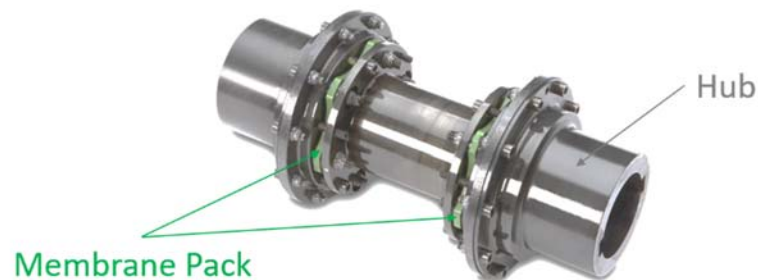


Figure 1.2 High Performance Disc Coupling (Reprinted from [4])

Coupling guard is a piece of equipment that encloses coupling to protect personnel from the rotating coupling. Figure 1.3 show a coupling guard that encloses

coupling. The heating of coupling guards and pressure distribution within coupling guards are closely associated with windage effects. According to API 671, maximum coupling guard temperature should not exceed 140°F (60 °C) [5], the investigation of coupling guard heating is therefore of practical significance.

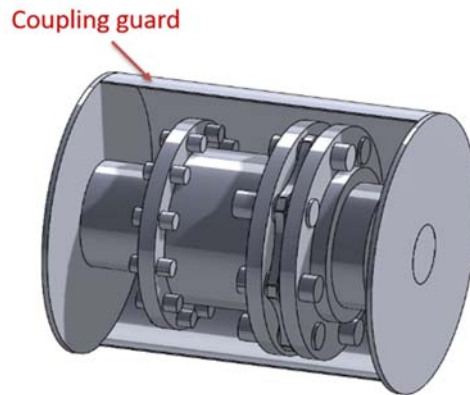


Figure 1.3 Coupling and Coupling Guard

In the presented research, Multivariable Regression Formulas (MRF) are developed based on CFD simulation results. Given the parameters related with a coupling guard or a gear, the formulas can be used to estimate coupling guard temperature or gearbox WPL. The formulas are developed based on linear regression and data used to generate the regression model is obtained from simulation experiments in CFD solvers (ANSYS CFX/ Fluent).

1.2 Literature review

Coupling enclosure, also known as coupling guard, is a piece of equipment that encloses rotating coupling. As shown in Figure 1.4, coupling connects motor drive and compressor. Coupling enclosure has a close clearance with coupling and used to protect personnel from the rotating coupling, whose rotating speed can be as high as 10000 rpm.

It was successfully used with oil lubricated coupling (e.g. gear coupling) for many years. However, after dry metal membrane couplings were installed in the enclosures high temperature was discovered on these enclosures [6].

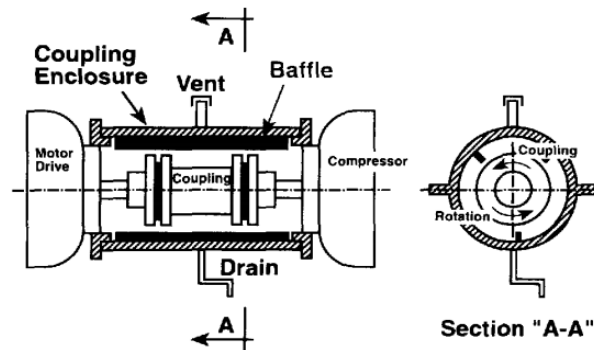
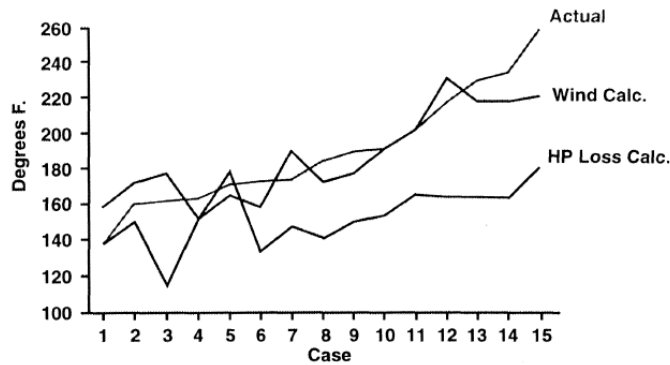


Figure 1.4 Coupling and Coupling Enclosure/Guard (Reprinted from [6])

The heat sources were identified as heat generated by air shearing and air turbulence. Calistrat introduced several methods to cool down the enclosure temperature and proposed an empirical formula [7] to predict coupling guard temperature where there is no air cooling provisions. A revised formula which included air cooling effect was later proposed [8]. Equations in the revised formula was use to write a temperature

prediction program (Wind). Figure 1.5 shows a comparison between actual guard temperature and predicted values from Wind calculations. If not considering highest and lowest temperature, an $\pm 10\%$ error was reported when comparing predicted values with test results from 15 case studies [9].



**Figure 1.5 Temperature Prediction by Revised Formula (Wind) and Comparison
(Reprinted from [9])**

Several methods have been developed to address the overheating problem of coupling guard. Adding windage flange is a common practice in industry with the purpose to reduce windage within coupling guard and therefore reduce guard temperature. With rotating bolts shielded, it is hoped that heat generated from air churning can be reduced. Figure 1.6 highlights windage flange on a coupling. However, tests and simulations carried out by Pennington and Meck [10] cast doubt on the effectiveness of the features. Their simulation results show that the addition of windage flange has little effect in reducing guard temperature.

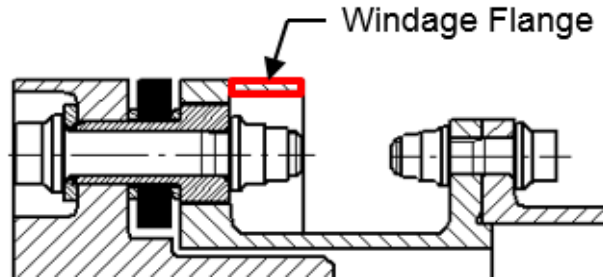


Figure 1.6 Section View of Coupling with Windage Flange (Reprinted from [11])

CFD method has also been used to help analyze field problems where coupling guard heating causes significant oil misting from coupling guard breather vent. Figure 1.7 shows coupling guard used on a turbo expander. The CFD predicted temperature ranges from 209 to 227°F, compared with measured temperatures from 219 to 222°F. Approaches to mitigate coupling guard heating are also provided [12].

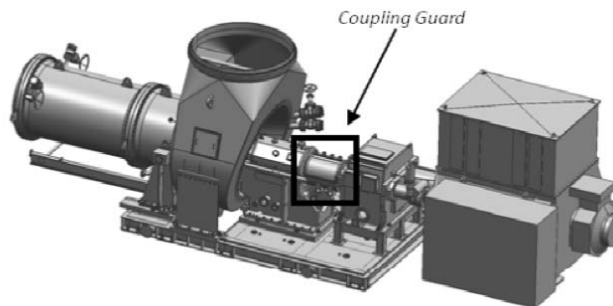
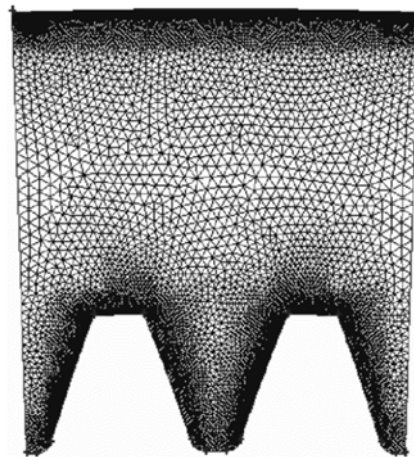


Figure 1.7 Coupling Guard on a Turbo Expander (Reprinted from [12])

Gear WPL has been investigated by both experiments and CFD approaches. Dawson [13] was among one of the first researchers to investigate gear WPL, he

conducted several experiments and deduced an empirical formula for WPL prediction. Y. Diab, et al. [14] carried out experiments to measure windage losses for spur gear rotated up to 12000rpm and proposed two analytical formula for windage losses prediction. His later research [15] determined that windage is prominent for high speed wide-faced gear units.

A two-dimensional CFD study of WPL from a single spur gear rotating in the air was conducted and simulation results compared reasonably well with test results. Figure 1.8 shows the mesh used in CFD simulation of a two-dimensional gear model. It can be seen that mesh close to the gear teeth and shroud is finer than that in other computational regions. Factors that influenced the gear WPL were identified using two-dimensional model in [16].



**Figure 1.8 Mesh for Gear Teeth with 5mm Peripheral Shroud
(Reprinted from [17])**

Due to the limitations of two-dimensional model, full three-dimensional model study was conducted and good agreement was obtained between simulation and test results [18-20]. Figure 1.9 showed a close match between numerical and experimental results. The numerical model was a three-dimensional spur gear tooth; periodic boundary condition was used so that only one gear teeth needs to be modelled.

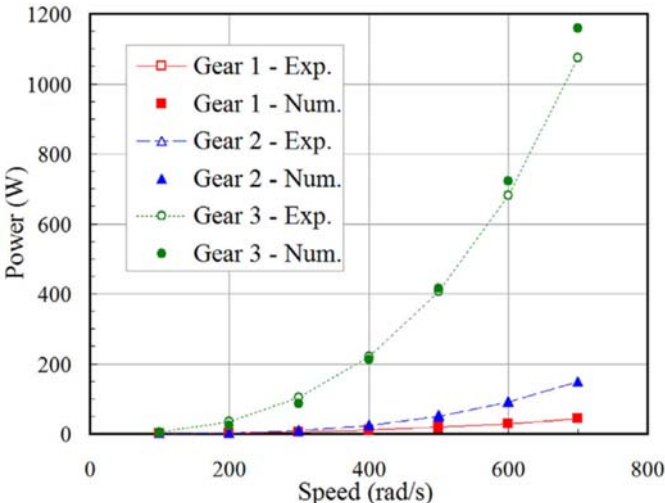


Figure 1.9 Experimental and Numerical Windage Power Loss (Reprinted from [18])

WPL from a single helical gear rotating in the air was also predicted using CFD approach [21, 22]. Figure 1.10 showed the computational domain of a helical gear tooth, only the gear tooth region was modelled. WPL generated by the rest of the region is estimated based on empirical formula proposed by the author.

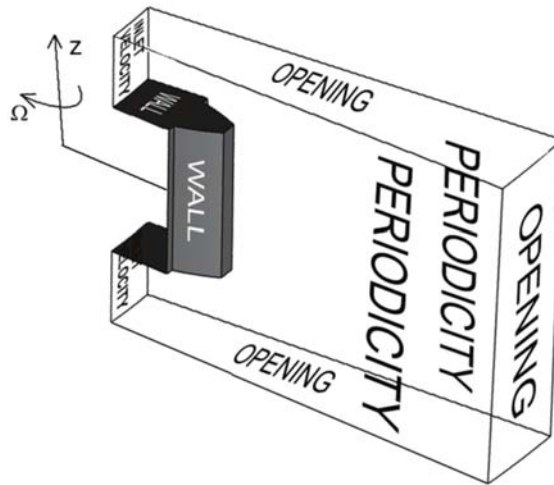


Figure 1.10 Numerical Domain and Boundary Conditions for Helical Gear WPL Simulation (Reprinted from [22])

Aerodynamic of gear windage loss has been studied by Matthew Hill, et al. [23]. A full-scale spur gear CFD model was built and solved by their own CFD code. The simulation results showed good agreement with the experiment.

WPL within gearbox was incorporated with churning and squeezing power loss. The sum of these losses was called hydraulic power loss. Preliminary simulation results showed good agreement with experimental results. Figure 1.11 showed velocity streamline of two meshing gear in a gearbox filled with oil [24]. Churning loss of rotating gear in gearbox was also modelled and velocity contours were plotted. The gear was half-immersed in the gearbox, a transient simulation was conducted using an open-source code [25].

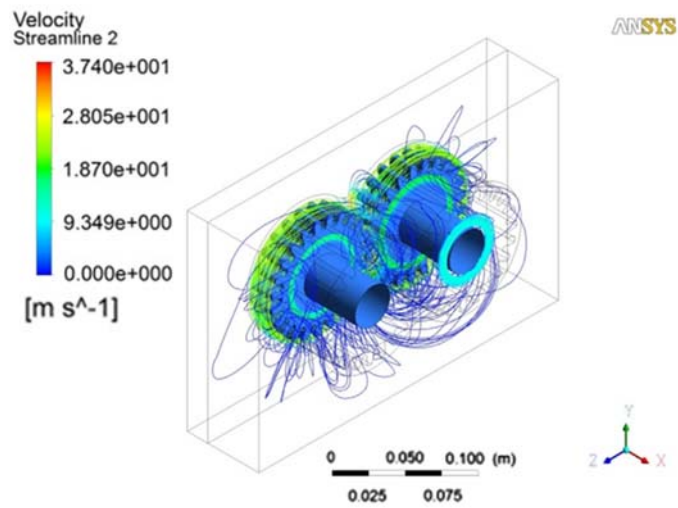


Figure 1.11 Velocity Streamline of Two Meshing Gear (Reprinted from [24])

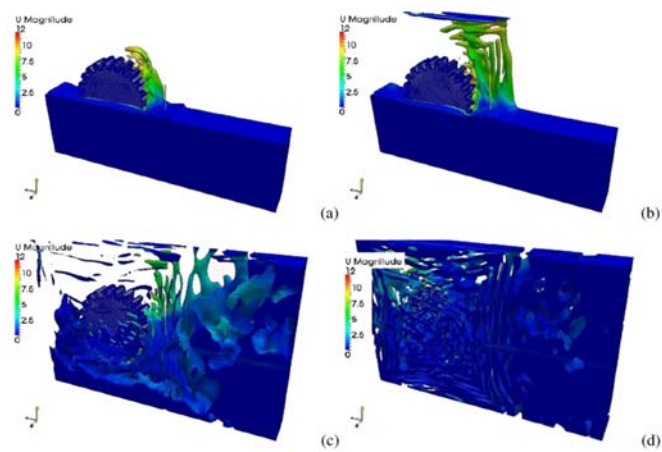


Figure 1.12 Velocity Contour of the Lubricant Within Gearbox (Reprinted from [25])

1.3 Research objectives

The presented research aims to develop Multivariable Regression Formulas (MRF) for the prediction of coupling guard temperature and gearbox WPL. Research objectives are listed below:

1. Validate CFD models of gears and coupling guards with experimental data in open literature;
2. Develop MRF and demonstrate that these formulas are accurate for coupling guards and gears that were not included in the CFD modeled systems which were used to generate the data for obtaining the MRF;
3. Identify optimal approach to select sets of parameter values for simulation experiments that saves computational cost, i.e. use minimal number of parameter sets, with high accuracy of the MRF (Accuracy here refers to yielding accurate results for systems that were not included in those that the MRF are based on);
4. Identify factors that will lower gear WPL and coupling guard maximum temperature.

2 COUPLING GUARD TEMPERATURE AND WINDAGE POWER LOSS: A CASE STUDY*

2.1 Problem description

High temperatures inside coupling guards can cause machinery down time and revenue loss. Adding a shroud (windage flange) around bolt heads is considered an effective method of reducing guard temperature. However, current studies have cast doubt on the effectiveness of this feature. If windage flanges are proved ineffective in reducing heat generation, removing them has huge potential to reduce churning losses, increase efficiency and reduce customers' energy costs related to turbomachinery. In addition, if the windage flanges are found to be ineffective, coupling manufacturing costs can be potentially reduced.

In this study, we validated CFD analysis through physical testing and used it to predict coupling guard temperature. We first investigated the effectiveness of windage flanges. The effect of guard radial clearance on guard temperature was also studied.

We hope to use CFD model to validate other windage mitigation features and provide guidelines for future anti-windage structure designs.

*Part of this section is reprinted with permission from "Coupling Guard Temperature and Windage Power Loss: CFD Analysis and Experiments," by A. Thompson, T. Zhai, A. Palazzolo, and A. Keshmiri, Proceedings of the Forty-fifth Turbomachinery Symposium, Houston, Texas, 2016.

2.2 Physical testing

2.2.1 Test configurations

A total of 6 configurations (Table 2.1) were designed in order to study the effectiveness of the windage flange and the effect of different radial clearance (Small: 20mm, medium: 40mm, large: 60mm) on guard temperature.

Table 2.1 Physical Test Configurations (Reprinted with permission from [11])

NO. of test configurations	Windage flange (Yes or No)	Size of coupling guard
1	Yes	Small
2	No	Small
3	Yes	Medium
4	No	Medium
5	Yes	Large
6	No	Large

Test configuration 5 was physically tested on the dynamic test rig and used to validate the CFD model. The remaining CFD models were set up as per the validated model. Physical testing of the remaining test configurations is planned to be carried out in order to further assess the accuracy of the CFD models, in an effort to create a model setup philosophy that can be used for predicting guard temperature.

2.2.2 Test rig overview

The test rig setup for the non-windage coupling with medium guard configuration is shown in Figure 2.1 (Guard cylinders removed for viewing purposes). The test rig capability allowed for a surface speed of 175m/s to be reached on the test coupling OD. Two annulus plates were mounted onto the stationary housing of the test rig, together with the diameter-variable cylinder halves that make up the coupling guard. The cylinder halves allowed for a variable radial clearance (From the coupling OD to the guard ID) of 20mm, 40mm and 60mm.

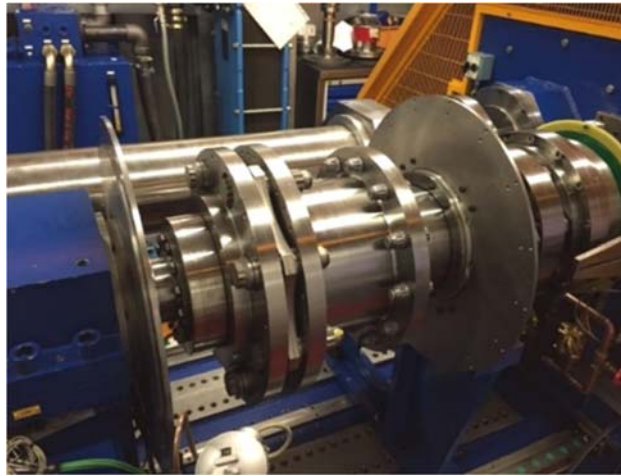


Figure 2.1 Test Rig Overview (Reprinted with permission from [11])

2.2.3 Temperature and pressure measurement

Temperature and pressure within the guard were measured by thermocouples and pressure transducers installed in the coupling guard cylinders. The location of the thermocouples and pressure transducers, as shown in Figure 2.2, were determined from initial CFD analysis which located hotspots within the guards.

During physical testing the test rig was run at the specified test speed of 7,500 rpm until steady state temperature in the guard was reached (After about 8 hours) and held to within $\pm 0.1^{\circ}\text{C}$ for an hour, at which point the values for all measurement devices were recorded and the test ended.

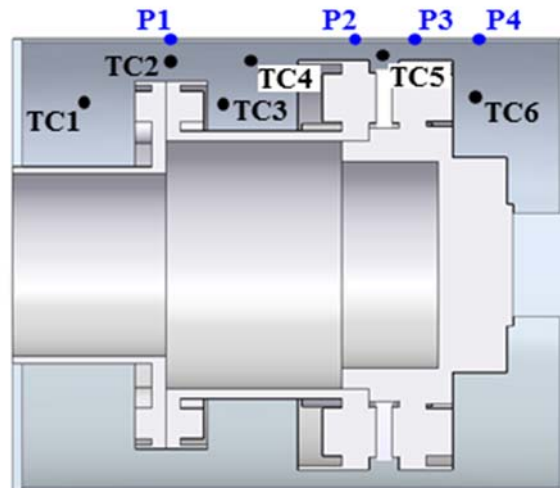
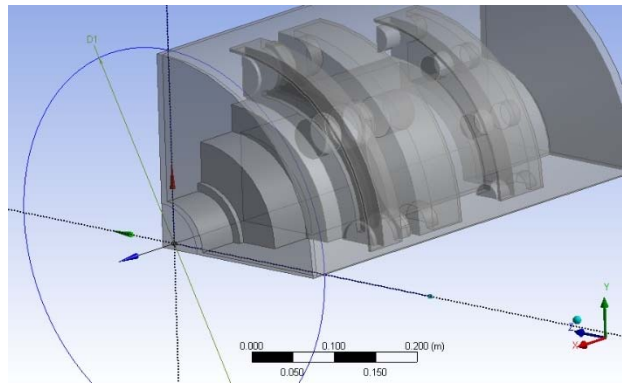


Figure 2.2 Location of Thermocouples (TC1 to TC6) and Pressure Transducers (P1 to P4) (Reprinted with permission from [11])

2.3 Steady state simulation in ANSYS CFX

2.3.1 Computational domain and mesh

In order to reduce computational time and aid solution convergence within CFX, a number of simplifications were made to the coupling and guard assembly to remove any unnecessary complex geometry. The model was reduced to a 1/4 section of the full model (Figure 2.3), and periodic boundary conditions were employed in order to reduce computational time.



**Figure 2.3 A 1/4 Section of Computational Domain
(Reprinted with permission from [11])**

The mesh was generated with four domains in order to reflect the realistic physical conditions. All four domains are shown in Figure 2.4. There are two fluid domains and two solid domains. Fluid domains modeled the fluid in-between the coupling and guard (Shroud) and the fluid inside the coupling. The material in the fluid domains was set to air with the density specified as ‘ideal gas’ for simplicity (Follows

ideal gas law). The rotating coupling domain and stationary guard domain are modeled, which allows for full heat transfer analysis of the solid bodies. The material for the solid bodies was set to steel.

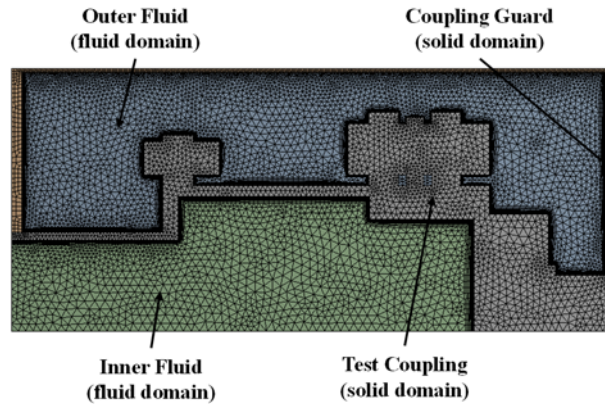


**Figure 2.4 Cross Section of Mesh Showing Four Domains
(Reprinted with permission from [11])**

Solid models of all six test configurations were built for the test coupling (with and without windage features) with variable radial clearances of 20mm, 40mm and 60mm as shown in Figure 2.5.

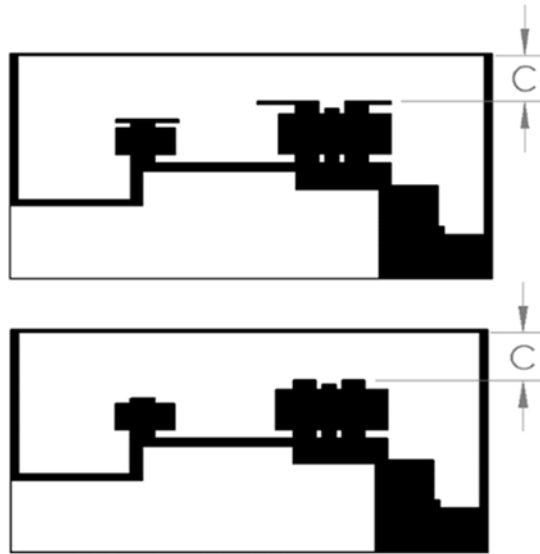


**Figure 2.5 Radial Clearances of Coupling Guard (C=20mm, 40mm and 60mm)
(Reprinted with permission from [11])**

2.3.2 Boundary conditions

Boundary conditions were imposed within CFX to reflect the physical conditions as closely as possible. Since the inner-fluid domain is connected with the other side of the spacer, outside of the test domain (Not shown in the figure). The air in the hollow of the coupling must be free to flow in or out of the domain. Therefore, an opening boundary condition with 140°F (60°C) inlet air temperature was imposed at this location.

In addition, as a result of recorded test data, a steady state temperature of 140°F (60°C) was also set on the right guard face to represent the temperature of the shaft. Thermal boundary conditions on both sides of the guard were assumed to be constant at

a temperature of 160°F (70°C). This is due to the test rig housing and shaft temperature having an influence on the temperature of the guard.

Significant heat is dissipated by natural convection through the coupling guard to atmosphere, and it is therefore crucial to determine the heat transfer coefficient of the guard solid body accurately. Assuming that the natural convection of the coupling guard resembles that of a horizontal cylinder [26], after some manipulations the correlation below was derived. The heat transfer coefficient was then imposed as a function of the temperature difference within the CFX-Pre setup.

$$\bar{h} = 1.229(T_{ave} - T_a)^{0.333}$$

Where,

\bar{h} Heat transfer coefficient, W/m²K

T_{ave} Volume average temperature of coupling guard, K

T_a Ambient temperature, set at 80°F (27°C)

A summary of the boundary condition details imposed on the model is illustrated in Figure 2.6.

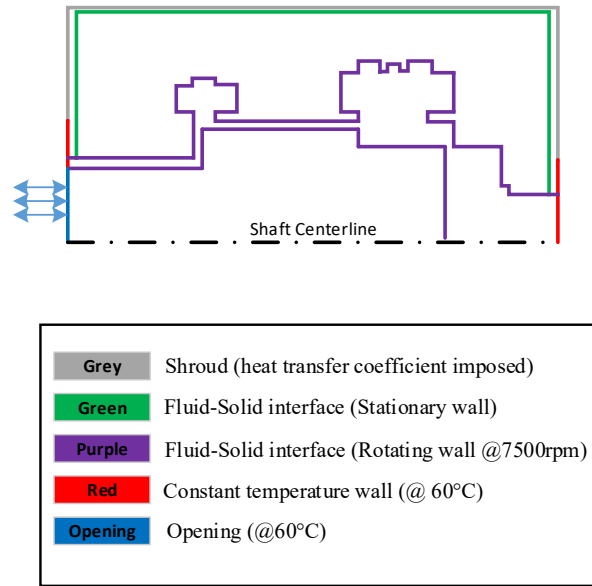


**Figure 2.6 Boundary Conditions of CFD Model
(Reprinted with permission from [11])**

Simulations of all six models were run until the solution was deemed to have converged approximately 3000 iterations. Convergence was determined when residual values were deemed to be sufficiently small (Less than 10^{-4}), and monitored volume averaged temperature results remained at a constant amplitude.

SST-k-omega turbulence model is used, as the flow is expected to be turbulent. Reynolds number Re can be calculated:

$$\text{Re} = \frac{VD}{\nu} = \frac{160 \times 0.438}{20 \times 10^{-6}} = 3.504 \times 10^6$$

Where

V Maximum velocity of coupling, m / s

D Characteristic diameter, m

ν Kinematic viscosity, m^2 / s

2.3.3 Simulation results

Validation of CFD simulation results against physical test results

The CFD model based on test configuration 4 was built, and the following temperature (With 2D streamline overlay) and pressure plots were generated in ANSYS CFD-Post. The simulation results from Figure 2.7 show that the temperature range within the guard is between 141°F – 245°F (61°C – 118°C) with the higher temperatures located in an area along the full length at the top of the guard. The streamline plot shows that large circulation patterns distribute air from the large coupling OD along the full length of the guard to the left and right guard faces.

When the coupling is rotating, along each cutline (Indicated in red), the speed of air close to the shaft is the highest and should generate the majority of heat. Therefore, area close to the rotating shaft should observe higher temperature than that at other points along the line. However, due to the heat dissipation within the coupling guard, hot air from other area can transport to the adjacent area and this cause a relative uniform air temperature across the region. Hot air from guard maximum diameter may heat the air at adjacent region and this result in a higher temperature of air further to the shaft.

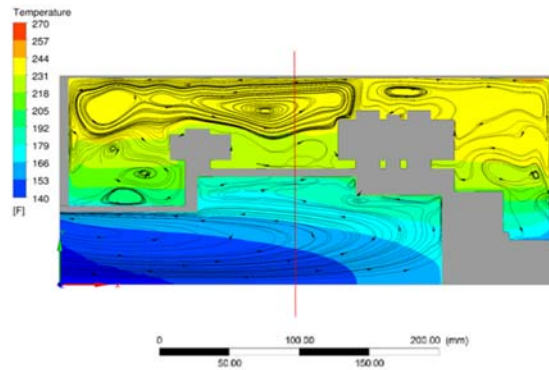


Figure 2.7 Temperature Contour Plot with 2D Streamline Overlay for Configuration 4: Medium Size Guard Without Windage Flanges (Reprinted with permission from [11])

Air circulation within the guard enhances turbulence and mixing of the air, subsequently heating or cooling the surrounding air. Figure 2.8 shows that the hottest part of the coupling is located at the large diameter flanges, and therefore the observed circulation patterns allow for this heat to be circulated effectively along the full length of the top area of the guard. The circulation gives a uniform temperature band along this area. It can be seen that the areas in the guard closer to the coupling do not reach the same temperature as at the OD, and that a uniform temperature within the entire inner-guard is not achieved. The streamline plot shows that this is due to the air flow circulation not extending into these areas.

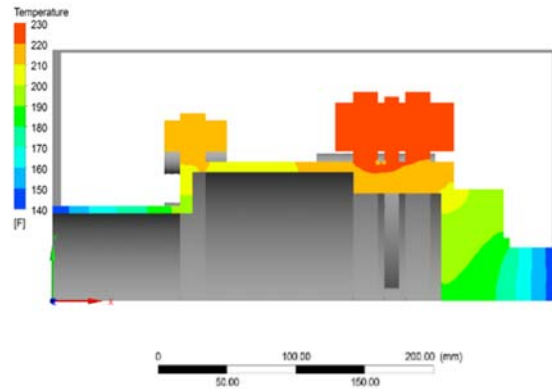


Figure 2.8 Coupling Temperature Contour Plot for Configuration 4: Medium Size Guard Without Windage Flanges (Reprinted with permission from [11])

A one-on-one comparison between simulation results and physical test data is shown below in Table 2.2 and Figure 2.9. The close match between experimental and simulation data (<5%) and analysis of the plots above, validates that the current CFD model setup is accurate and therefore justifies the decision to model the remaining configurations based on similar procedures.

Table 2.2 Comparison Between Test and Simulation for Test Configuration 4 (Reprinted with permission from [11])

No. of Thermocouple	Location (in CFD Model)			Medium Guard, Non-windage Features		Percentage Difference
	X / mm	Y / mm	Z / mm	Test Data/ °C (± 0.1°C)	Predicted Temperature/ C°	
TC 1	77	172	0	112.1	108.8	-3.0%
TC 2	169	228	0	116.1	113.3	-2.5%
TC 3	225	169	0	115.5	107.1	-7.2%
TC 4	339	239	0	119.6	113.4	-5.2%
TC 5	397	234	0	117.4	115.9	-1.3%
TC 6	495	177	0	116.1	112.7	-2.9%
	Average			116.1	111.9	-3.6%

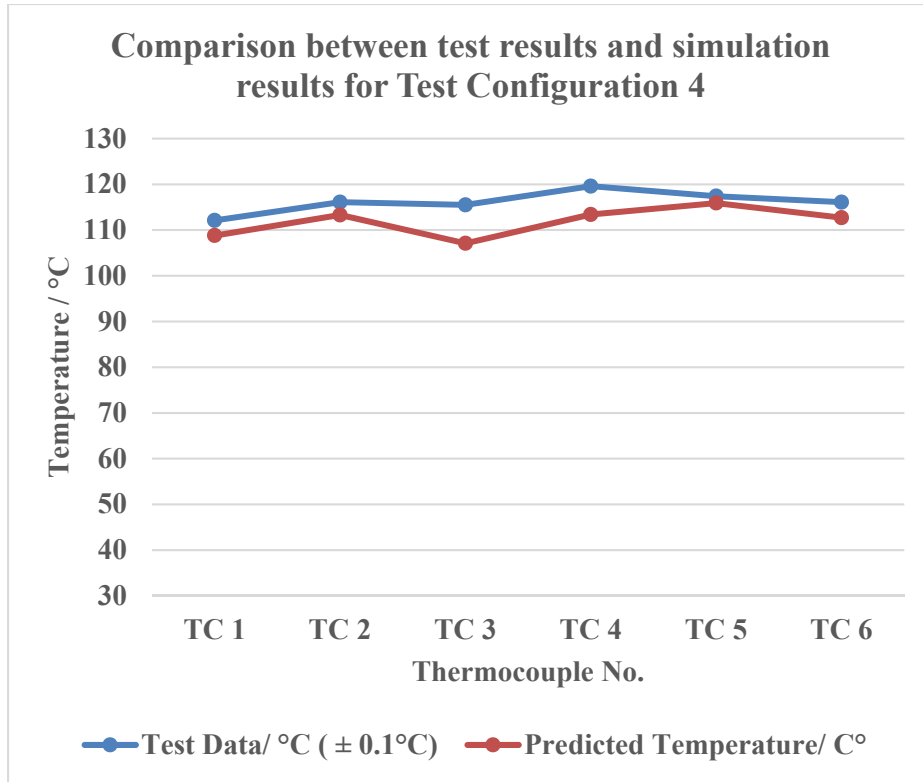


Figure 2.9 Comparison Between Simulation Results and Physical Test Results for Test Configuration 4: Medium Guard Without Windage Flanges (Reprinted with permission from [11])

Simulation results for all six test configurations are listed in Table 2.3, description for each result is followed.

Table 2.3 Contours in CFD-POST and Analysis

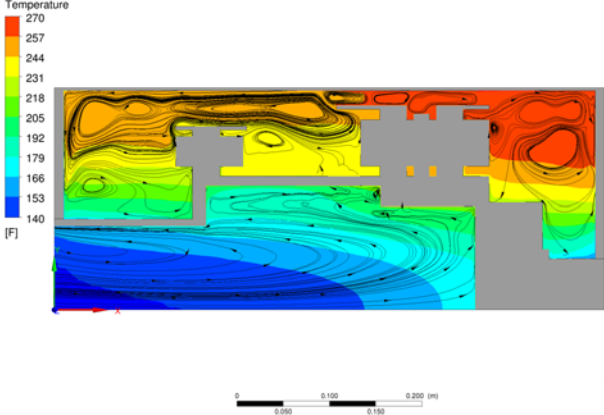
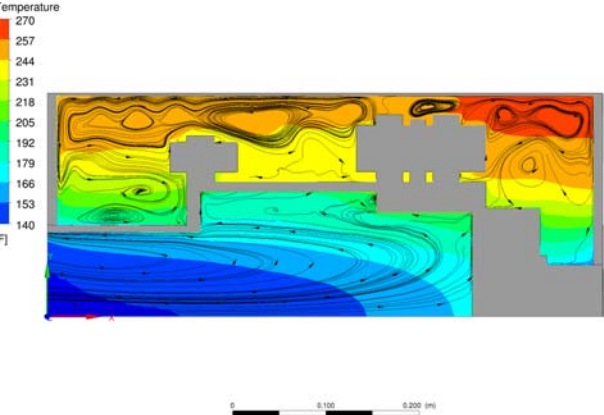
Test No.	Temperature contour plot with 2D streamline overlay	Description
<p>1 (Small guard, with windage flange)</p>		<p>With windage flanges added, the temperature within the coupling guard is not reduced.</p> <p>Compared with Test 2, maximum temperature increased by 7°F (4°C)</p>
<p>2 (Small guard, without windage flange)</p>		<p>Air circulation in the guard, changes with the addition of the windage flanges.</p> <p>The large circulation pattern to the left is cut short to some extent by the windage flange geometry, and is not able to circulate heat generated by the windage flanges to this area as effectively.</p>

Table 2.3 Continued

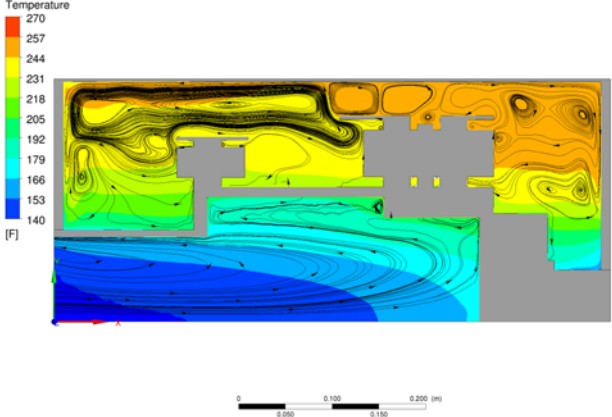
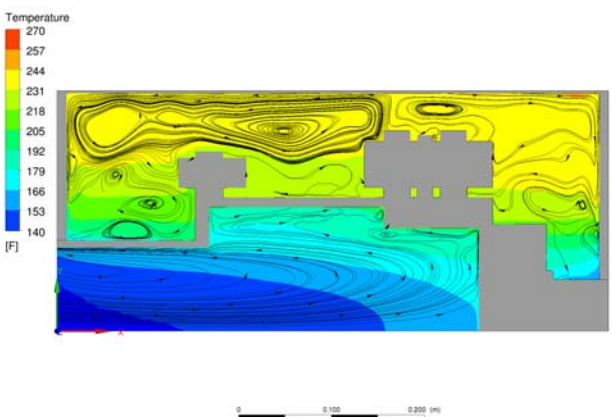
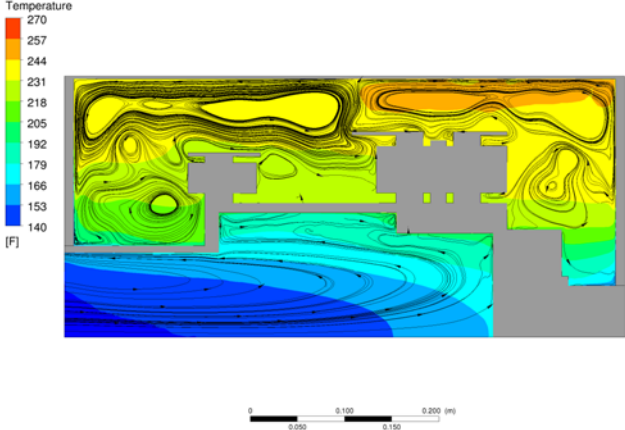
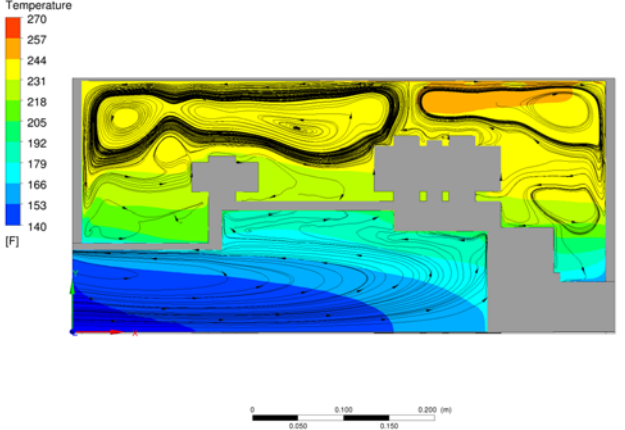
Test No.	Temperature contour plot with 2D streamline overlay	Description
<p>3 (Medium guard, with windage flange)</p>		<p>With windage flanges added, the temperature within the coupling guard is not reduced.</p> <p>Compared with Test 4, temperature within the guard is 141°F – 257°F (60°C – 125°C) which shows maximum temperature increased by 12°F (7°C)</p> <p>Air circulation in the guard, changes with the addition of the windage flanges.</p>
<p>4 (Medium guard, without windage flange)</p>		<p>The large circulation pattern to the left is cut short to some extent by the windage flange geometry and is not able to circulate heat generated by the windage flanges to this area as effectively.</p>

Table 2.3 Continued

Test No.	Temperature contour plot with 2D streamline overlay	Description
<p>5 (Large guard, with windage flange)</p>		<p>With windage flanges added, the temperature within the coupling guard is not reduced.</p> <p>Compared with Test 6, maximum temperature doesn't change significantly</p>
<p>6 (Large guard, without windage flange)</p>		<p>Air circulation in the guard, changes with the addition of the windage flanges.</p> <p>The large circulation pattern to the left is cut short to some extent by the windage flange geometry, and is not able to circulate heat generated by the windage flanges to this area as effectively.</p>

2.4 Lessons learned

The simulation results for all 6 configurations showed that the windage flanges fail to effectively reduce temperature within the coupling guard and therefore could not reduce the guard surface temperature. This was because the addition of windage flange increased surface area at maximum guard diameter. The friction between air and the increased surface area caused more heat generation and temperature within coupling guard was therefore increased.

We also learnt that with the increase of radial clearance, there seemed to exist a point (Between 40 and 60mm) after which the windage flange had little effect on the temperature within the coupling guard.

The CFD model can provide accurate simulation results, as validated by test results. With the test results from other configurations become available, a more robust model can be developed. While current CFD model was built based on R&D test results, the simulation technique and boundary condition setup could be used for temperature prediction of different types of coupling enclosures.

Practically speaking, to build CFD model for each different case is time consuming. It is therefore of interest to develop a generic model, based on which the effect of parameters can be studied by extensive CFD simulation. A mathematical model can then be proposed for future prediction. The mathematical model is usually a regression based model. With careful design of simulation experiments, the correlation between input and output parameters can be obtained with minimum simulation runs.

We will discuss the development of such a regression model for coupling guard temperature prediction in next section.

3 REGRESSION MODEL FOR COUPLING GUARD TEMPERATURE PREDICTION

3.1 Calistrat's empirical formula for temperature prediction

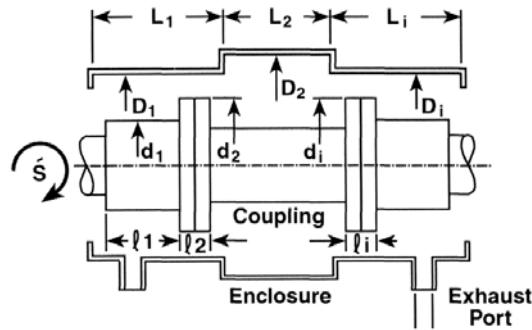


Figure 3.1 Input Parameters in Calistrat's Empirical Formula (Reprinted from [9])

Figure 3.1 shows parameters used in Calistrat's empirical formula to predict temperature. Coupling and coupling guard geometry, temperatures, rotating speed are taken into consideration. Final form of the expression is shown below:

$$T_c = K_2 K_3 K_4 \left(\frac{cpm}{1000} \right)^{(1.8/K_1)} + (T_a + T_{shaft}) / 2$$

Where,

T_c Coupling temperature, °F

T_a Ambient temperature, °F

T_s Shaft temperature, °F

$$K_1 = \left(\frac{\text{Enclosure Diameter}}{\text{Maximum Cooling Diameter}} \right)^{0.27}$$

$$K_2 = \frac{[(D_1^{2.8})(L_1)] + [(D_2^{2.8})(L_2)] + [(D_3^{2.8})(L_3)] + \dots}{\text{Enclosure Surface Area}}$$

$$K_3 = \left(\frac{\text{Maximum Coupling Diameter}}{\text{Minimum Colling Diameter}} \right)^{0.2}$$

$$K_4 = 0.6$$

The formula has 2 main components, first component contains parameters K_1 , K_2 , K_3 , K_4 which describes the effect of coupling geometry. $K_4 = 0.6$ indicates that there are no provisions for air circulation. The coupling is regarded as a combination of cylinders with different diameters. Particular attention is paid to the maximum coupling diameter where highest speed occurs. However, the formula ignores the effect of bolt heads. The number of bolt heads may affect the windage effect within enclosure and therefore change the enclosure temperature.

The other component in the formula is the average of shaft temperature and ambient temperature. CFD analysis shows that the temperature of shaft inlet portion has a direct influence on the temperature within enclosure. In terms of ambient temperature, it is assumed ambient temperature to be constant with air conditioning. Initial data analysis (Ambient temperature from 60°F to 100°F) also shows that ambient temperature is not statistically significant.

Note that the above formula is used to calculate coupling temperature. In order to obtain the temperature of enclosure, following formula is used:

$$T_e = 0.85T_c + 10^\circ F$$

Where,

T_c Coupling temperature, °F

T_e Enclosure temperature, °F

3.2 Multivariable regression formulas for temperature prediction

3.2.1 Baseline model for simulation

A baseline model is built as shown in Figure 3.2. The geometry of the coupling is depicted in Figure 3.3. This is a disk coupling with 20 bolts on each flange and operates at 5400 RPM. There is a driving unit (Gas expander turbine) and a driven unit (Gearbox) on each side of the coupling.

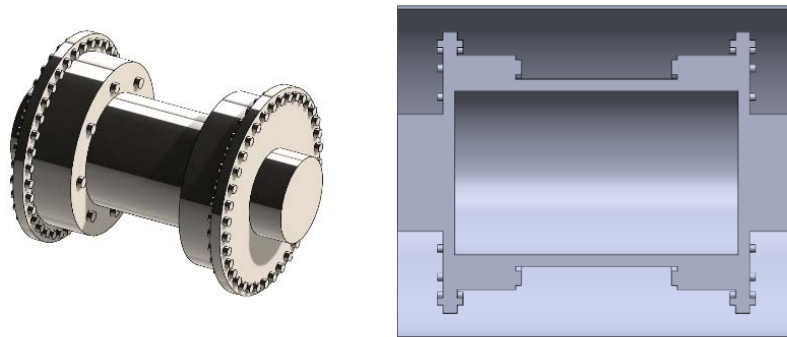


Figure 3.2 Coupling Geometry and Cross Section View with Coupling Guard

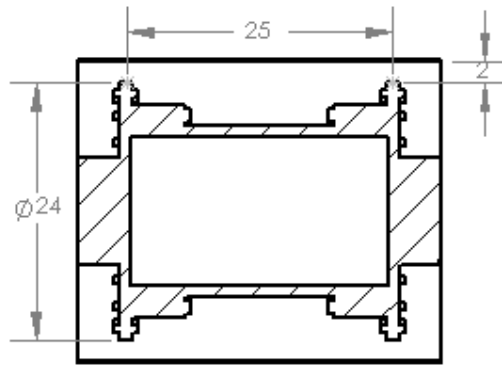


Figure 3.3 Key Dimensions of Computational Domain

The input parameters for this baseline model is listed in Table 3.1, this parameter set is later numbered as No.10 in the Design of Experiments.

Table 3.1 Input Parameters for Initial Simulation

DBFF (inch)	Rotating speed (rpm)	Max Diameter (inch)	Radial Clearance (inch)	Shaft Temperature (°F)	Ambient Temperature (°F)	No. of bolts
25	3600	24	2	120	100	20

3.2.2 *Choice of parameters*

Regression model is intended to predict maximum guard temperature for couplings in special-purpose applications. These applications usually referred to large and/or high speed machines, in the services where operating for extended periods is required. [5]

To choose relevant parameters and their ranges are the most important step before conducting simulation experiments. While there is no strict rule in choosing parameters, the scope of the API standard makes it clear that the parameters involved should be critical for special-purpose applications, and the ranges of these parameters should be reasonable for such applications.

Current choice of parameters and their ranges are based on the case study and geometry drawing provided by industry partners. Also, in Calistrat's empirical formula for coupling guard temperature prediction, a few geometry and temperature parameters are identified. In the proposed model, similar parameters are adopted.

Instead of dividing coupling into small cylinders and consider individual length and diameter, two 'characteristic length' are chosen. The parameters are to account for the effect of coupling geometry. Also note that air cooling effect is not included in current simulation. In addition, following assumption is made to eliminate number of parameters:

Assume that coupling enclosure is made of steel with a thickness of 0.24 in (6 mm) and the length is 34 inch (863.6mm). Also assume that inlet portion of the shaft has

a constant temperature. There are no active cooling provisions (Exhaust port, etc.) included in the simulation, therefore the heat transfer is mainly through the enclosure and shaft ends. Figure 3.4 shows the parameters included in regression based model.

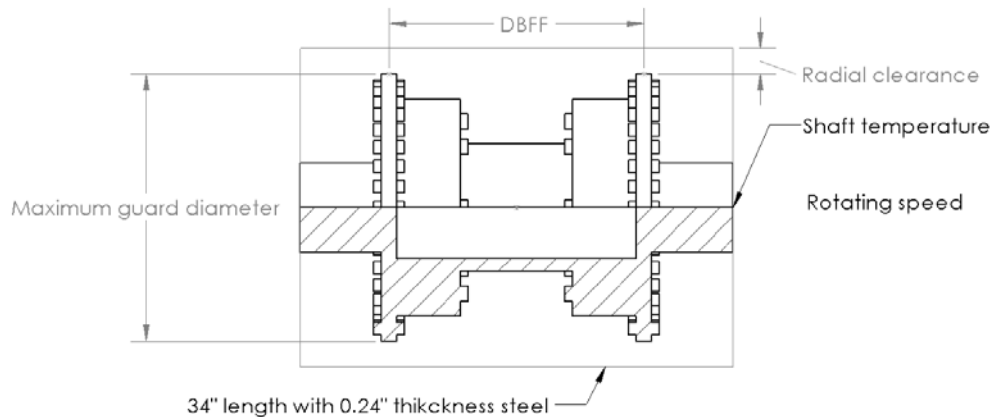


Figure 3.4 Parameters in Regression Based Model

Input parameters

1) Rotating speed: 3600-7200 rpm

Initial simulation shows that rotating speed has a profound influence on heat generation within enclosure. This effect intensifies quadratically as rotating speed increases. This is because with larger velocity gradient, friction will increase and it is a major source of heat generation.

2) Max coupling diameter: 18-24 inch

Maximum guard diameter is regarded as 'characteristic length' of coupling. Highest surface speed on coupling occurs at maximum diameter and highest temperature on coupling is expected. Therefore, it is an important indication of heat generation.

3) DBFF (Distance Between Flange Faces): 20-30 inch

DBFF is another 'characteristic length' of coupling which determines the relative location of flanges within enclosure. This value has the potential to alter air circulation within enclosure and therefore change temperature on guard.

4) Radial clearance: 1 - 2 inch

Radial clearance between coupling maximum diameter and enclosure inner surface is required to be at least 1". Windage effect, one of heat generation sources, is particularly strong between 1 inch and 2 inch.

5) Shaft temperature: 100 - 160 F

The heat transfer through shaft is an important path to dissipate heat and therefore will affect enclosure temperature. Calistrat suggested that shaft temperature can be estimated by the temperature of bearing oil.

6) Ambient temperature: 60 - 100 F

The ambient temperature will affect heat transfer coefficient (htc) on enclosure (htc is imposed as a function of ambient temperature and area averaged surface temperature). Depends on whether the facility is indoor or outdoor, an estimate range of ambient temperature is given.

7) Number of bolts on coupling flanges: 12-36

The bolt heads are evenly distributed across the flange. Their rotating in trapped air will cause friction which is one of the major sources of heat generation.

Output parameters

1) Maximum surface temperature of coupling enclosure

This output is identified in API standards, as it is important for personnel safety and is an indication of whether the guard is overheating. It is the most important output parameter.

2) Torque on coupling

For high speed coupling, WPL is significant. WPL on coupling can be calculated from multiplying torque by angular velocity.

3) Minimum pressure in simulation domain

The oil suction past seals into the enclosure is due to the negative pressure near the shaft. This phenomenon is also observed from CFD simulation results. To locate the minimum pressure within domain and take actions to prevent oil suction due to negative pressure are therefore of interest. From the mesh independence study, the pressure value fails to stabilize after mesh refinement. Therefore, prediction expression is not provided for minimum pressure.

3.2.3 Simulation procedures

Solid modeling

Using dimensions from the baseline model, solid model of coupling and its enclosure are modeled in SolidWorks. Computational domain is divided as shown in Figure 3.5. Note that both fluid and solid regions are modeled to reflect actually physical settings. Fluid regions include area between coupling and coupling enclosure, solid regions are coupling and its enclosure.

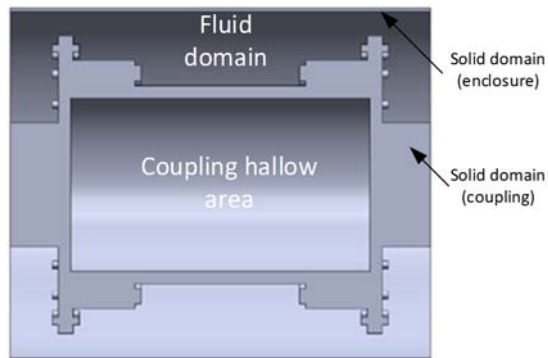


Figure 3.5 Computational Domain

Meshing and mesh independence study

Mesh is generated in ANSYS Meshing (Under ANSYS Workbench). In order to reduce computational time, a 1/4 section is modelled. In the regions close to the fluid-solid interface, inflation with smooth transition is used to ensure good mesh quality.

To ensure mesh independent results, mesh independence study is carried out. Three level of mesh density is taken into consideration: very coarse, coarse, fine and very fine. As the mesh become finer, we can find that monitored values are becoming stable (Except for minimum pressure). It is shown in Table 3.2 that coarse mesh is sufficient for current simulation, therefore similar meshing strategy is used for the rest of simulation cases.

Table 3.2 Mesh Independence study

Mesh	No. of elements/ ×10⁶	Volume average temperature/ °F	Maximum temperature/ °F	Windage torque/ ×4 Nm	Minimum pressure/ Pa
Very coarse	1.02	198.882	205.382	-2.02134	-2018 (2.0%)
Coarse	3.69	193.441	198.938	-1.64319	-3476 (3.4%)
Fine	6.40	193.211	198.575	-1.64944	-1093 (1.1%)
Very fine	10.36	192.886	198.247	-1.64509	-2197 (2.2%)

The 1/4 section of the whole model is meshed and shown in Figure 3.6. Periodic boundary condition is therefore used in CFX.

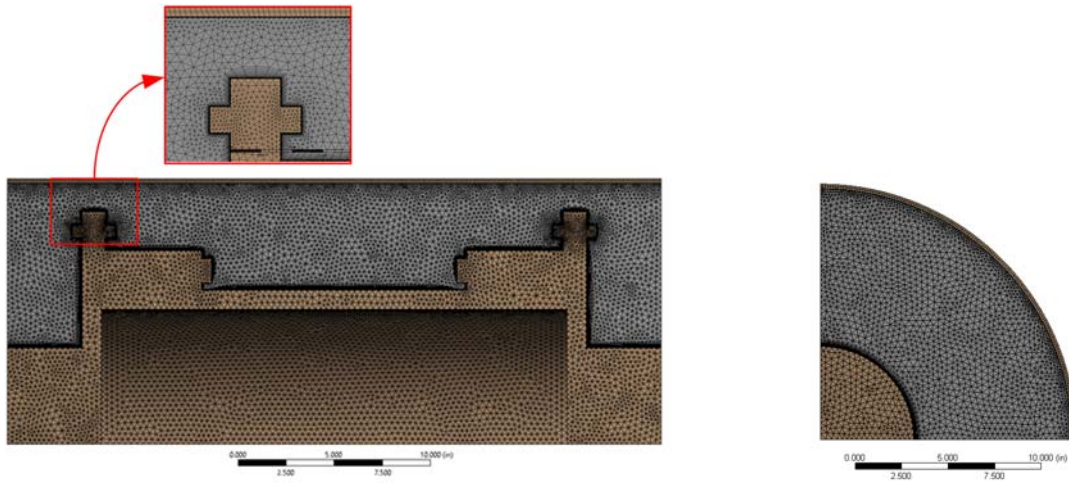


Figure 3.6 Mesh for 1/4 of the Computational Domain

Boundary conditions in CFX

Periodic boundary condition for all 3 domains is identified in Figure 3.7:

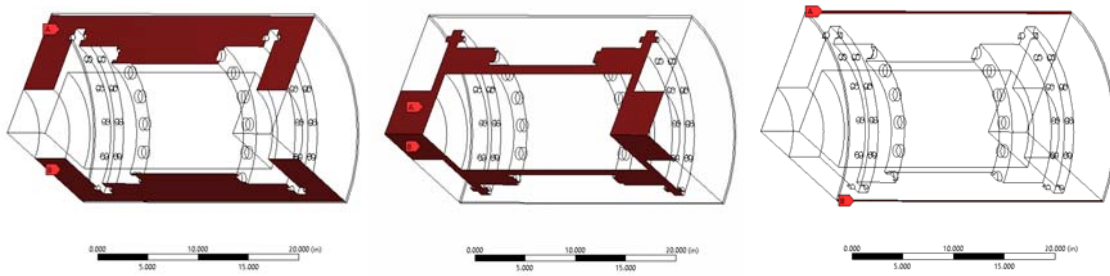


Figure 3.7 Periodic Boundary Conditions

Detailed description for each boundary condition in CFX is listed in Table 3.3.

Location for each boundary condition is highlighted and a unique name is given.

Table 3.3 Boundary Conditions in CFX

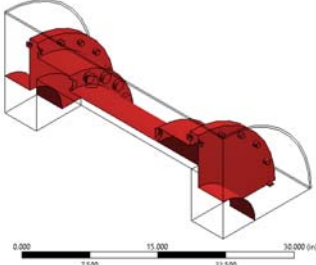
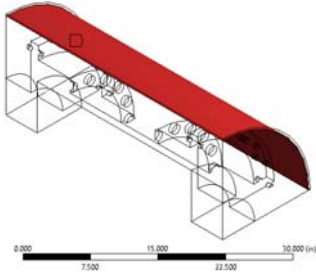
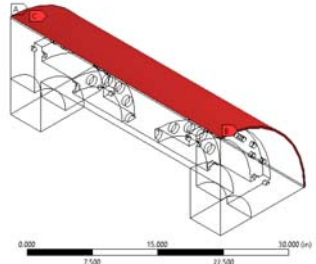
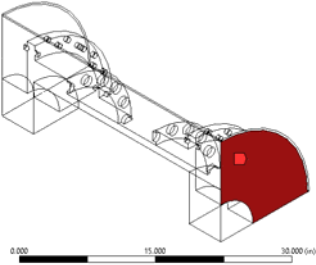
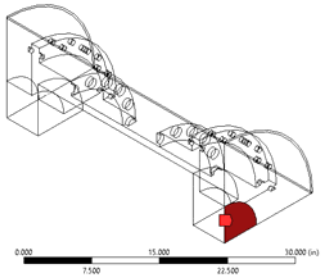
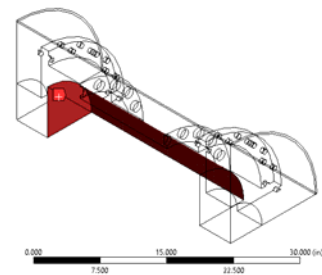
Location	Name	Description
	rotor_outerfluid	<p>Type: Fluid-solid interface (general connection) Interface between coupling and air within enclosure, domains on each side of the interface are rotating with the same angular velocity. Therefore, a general connection is imposed.</p>
	outerfluid_shroud	<p>Type: Fluid-solid interface (frozen rotor) Interface between air in rotating domain and stationary coupling enclosure. A counter-rotating wall is imposed on the fluid side of the interface. Frozen rotor method is used for the interface and pitch angle is specified as 90°.</p>
	shroud_htc, side 1, side 2	<p>Type: Wall (stationary) Outer surface of coupling enclosure where heat transfer coefficient and ambient temperature is imposed. The majority of the heat dissipate from the enclosure.</p>
	fluid_stationary1, fluid_stationary 2	<p>Type: Wall (counter-rotating) Locate at both ends of the coupling, so that coupling is fully enclosed. The same thermal boundary conditions for enclosure outer surface are imposed. Heat can also dissipate from these walls.</p>

Table 3.3 Continued

Location	Name	Description
	<p>shaft_inlet1, shaft_inlet2</p>	<p>Type: Wall They are shaft ends and a constant temperature is applied. To have a good estimate of this temperature is important, because heat can dissipate through the coupling to the shaft by conduction.</p>
	<p>innerfluid_wall</p>	<p>Type: Wall Inner surface of coupling hollow region, rotating with coupling.</p>

Since coupling guard is the main path for heat to dissipate, it is crucial to apply proper thermal boundary condition on the guard. Natural convection occurs on coupling guard and it is assumed that nature convection of coupling guard resembles that of horizontal cylinder.

Table 3.4 shows parameters in an empirical formula for natural convection. Rayleigh number (Ra) is first calculated. Based on the range of Ra , coefficients of the formula is chose from the table.

**Table 3.4 Proposed Correlation for
Natural Convection from Horizontal Cylinders (Reprinted from [26])**

Range of $(Ra)_{D,f}$		$(Nu)_{D,f} = B_1(Ra)_{D,t}^{m_1}$	
From	To	B_1	m_1
10^{-10}	10^{-2}	0.675	0.058
10^{-2}	10^{-2}	1.02	0.148
10^2	10^4	0.85	0.188
10^4	10^7	0.48	0.25
10^7	10^{12}	0.125	0.333

Rayleigh number (Ra) is defined as,

$$Ra_D = \frac{g\beta(T_s - T_a)D_c L^3}{\nu^2}$$

Where,

D_c Diameter of the coupling guard, mm

Ra_D Rayleigh number

g Acceleration due to gravity, $9.8m/s^2$

T_s Surface temperature, °F

T_a Ambient temperature, °F

ν Kinematic viscosity, m^2/s

β Thermal expansion coefficient (Equals to $1/T$, T is absolute temperature, °F)

$$\overline{Nu_D} = \frac{\bar{h}D}{k} = B_1 Ra_D^{m_1} = 0.125 Ra_D^{0.333}$$

After some manipulations, heat transfer coefficient is imposed as a function of temperature difference in CFX-Pre.

$$\bar{h} = 1.229(T_s - T_\infty)^{0.333}$$

Expression input for heat transfer coefficient in CFX-PRE:

$$1.229 \text{ W m}^{-2} \text{ K}^{-1} * \text{abs}((\text{areaAve}(T)@\text{shroud}/1 [\text{K}]-300[\text{K}]/1 [\text{K}]))^{(0.333)}$$

Post-processing in CFD-POST

After about 3000 iterations, convergence is reached. The simulation is performed on 20 cores of TAMU Supercomputer, the computational time for each case is about 7 hours.

Maximum temperature, minimum pressure and torque on coupling can be read from CFD-POST. A sample simulation results are listed in Table 3.5.

Table 3.5 Output Parameters for Sample Simulation

Max Temperature (°F)	Torque (Nm)	Min Pressure (Pa)	Power Loss (W)
195.9	-1.14	-504.2	429.8

Figure 3.8 shows temperature distribution on coupling guard. The contour is almost symmetry and highest temperature is observed close to the ends of coupling guard. These areas locate above the coupling flanges which have largest diameter.

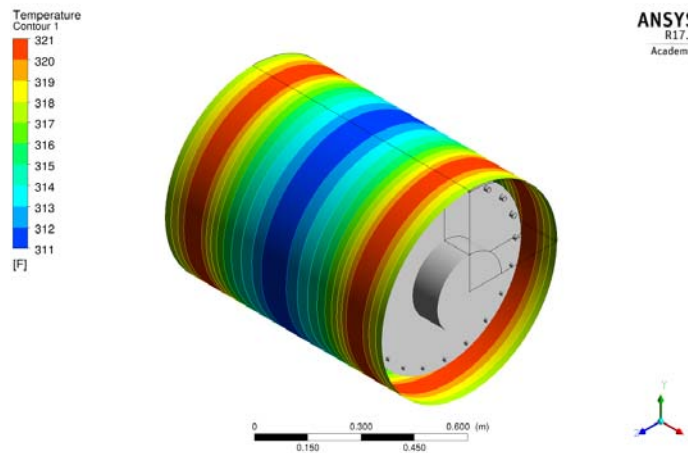


Figure 3.8 Temperature Contour of Coupling Guard

A temperature contour with velocity streamline overlay shows temperature distribution within the enclosure. Temperature in most area ranges from 309°F to 325°F,

with lower temperature close to the shaft ends. The effect of shaft temperature can be seen from Figure 3.9. Heat generated can conduct through the coupling, this is another path for heat dissipation.

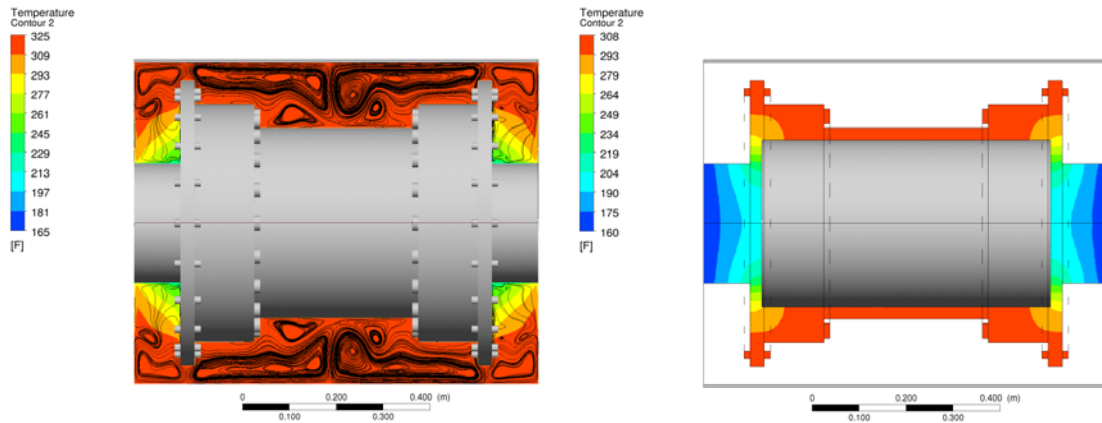


Figure 3.9 Temperature Contour within Coupling Enclosure and on Coupling

Negative pressure is observed in regions close to the shaft (Figure 3.10), this supports the notion of a negative pressure vacuum effect that present on large diameter couplings rotating at high speed as discussed by Carter [9]. It is stated that large diameter couplings have a higher surface speed that drives air radially outwards away from the shaft, creating a negative pressure zone that can cause oil suction past labyrinth seals.

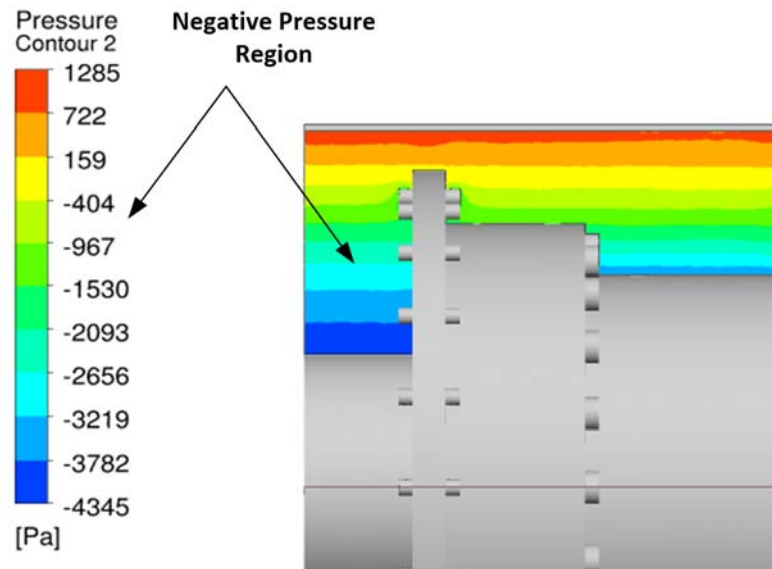


Figure 3.10 Negative Pressure Region Within Coupling Enclosure

3.2.4 Design of simulation experiments and results

Design of Experiment can help reveal relationships between factors and responses, it provide insights that cannot be obtained from sampling factors one at a time[27]. Simulation experiments are designed in JMP to allow for minimum number of runs. Response Surface Methodology (RSM) is used for the design of simulation experiments, where optimal response can be obtained using a sequence of designed experiments. There are 7 factors (Independent variables) and 3 responses (Dependent variables).

Custom Designer in JMP constructs a design based on the needs of users and nature of the problem. Factors and responses need to be specified by the users, this

includes the range for the continuous factors and responses. The Custom Designer allows a more efficient design which can save time and make better use of resources for conducting experiments. [28]

Initial simulation results show that ‘Rotating speed’, ‘Max diameter’ and their interaction terms are statistically significant. To minimize simulation runs, experiments are designed to emphasis the effects of above two terms.

Table 3.6 Design of Simulation Experiments and Results Reported in ANSYS CFX

No	DBFF* (inch)	Input parameters						Observed parameters			
		Rotating Speed (rpm)	Max Diameter (inch)	Radial Clearance (inch)	Shaft Temperature (°F)	Ambient Temperature (°F)	No. of Bolts	Max Temperature (°F)	Windage Torque (Nm)	Min Pressure (Pa)	Power Loss (W)
1	20	3600	18	2	180	60	20	171.41	-0.4	-1378.2	150.8
2	20	3600	24	1.5	120	80	36	205.6	-1.33	-2480.6	501.4
3	20	3600	24	2	180	60	20	206.5	-1.08	-2457	407.2
4	20	5400	18	1	120	80	28	208.54	-0.9	-3204.8	508.9
5	20	7200	18	1	180	100	36	343.89	-1.4	-4082	1055.6
6	20	7200	21	2	180	80	20	380.5	-2.38	-7195.4	1794.5
7	20	7200	24	1	180	80	36	548.6	-3.35	-6677.4	2525.8
8	20	7200	24	2	120	100	36	512.7	-3.48	-6025.8	2623.9
9	25	3600	18	2	120	100	20	284.83	-1.23	-5675.4	463.7
10*	25	3600	24	2	120	100	20	195.9	-1.14	-504.2	429.8
11	25	5400	18	2	120	80	36	200.7	-0.95	-3207.3	537.2
12	25	5400	21	1.5	150	100	28	278.2	-1.47	-4364.1	831.3
13	25	5400	24	2	120	60	20	294.3	-2.16	-1046.3	1221.5
14	25	7200	21	1.5	120	60	36	380.5	-2.38	-7199	1794.5
15	30	3600	18	1	180	80	36	185.72	-0.46	-1095.5	173.4
16	30	3600	21	2	120	60	20	149.92	-0.73	-2259.1	275.2
17	30	3600	24	1	180	80	20	219.1	-1.08	-2160.9	407.2
18	30	3600	24	2	180	80	36	224.9	-1.28	-2151.3	482.5
19	30	7200	18	1.5	180	80	20	284.83	-1.23	-5675.5	927.4
20	30	7200	24	1	120	100	20	462.9	-2.99	-6651.5	2254.4
21	30	7200	24	2	180	80	36	501.4	-3.43	-6263.1	2586.2

*Simulation No.10 is the baseline model

The simulation experiments are designed to reveal main effects and interactions between factors. Rotating speed, Max coupling diameter and their interactions are reported to be most statistically significant. The prediction expression is also available in JMP.

3.2.5 Regression-based model

The coefficients used for the formula is reported in JMP and final form of the expression is (Units of parameters in the expression is the same as those in Table 3.6):

$$\begin{aligned}
 \text{GuardT} = & 1.506\text{AmbientT} - 0.537\text{DBFF} + 19.457\text{Max_diameter} \\
 & + 0.311\text{No_bolts} - 6.591\text{Radial_clearance} + 0.051\text{Rotating_speed} \\
 & + 0.439\text{ShaftT} + (0.125\text{No_bolts} - 3.5)(5.856\text{Max_diameter} \\
 & - 122.987) - (0.033\text{ShaftT} - 5.0)(0.003\text{Rotating_speed} \\
 & - 21.273) - (0.05\text{AmbientT} - 4.0)(9.301\text{Max_diameter} \\
 & - 195.330) - (0.05\text{AmbientT} - 4.0)(0.006\text{Rotating_speed} \\
 & - 34.924) - (0.0333\text{ShaftT} - 5.0)(1.433\text{Max_diameter} \\
 & - 30.107) - (0.784\text{DBFF} - 19.605)(0.333\text{Max_diameter} - 7.0) \\
 & - (0.0005\text{Rotating_speed} - 3.0)(0.933\text{DBFF} - 23.328) \\
 & + (0.125\text{No_bolts} - 3.5)(0.007\text{Rotating_speed} - 39.015) \\
 & - (2.0\text{Radial_clearance} - 3.0)(0.003\text{Rotating_speed} - 21.049822) \\
 & - (13.306\text{Radial_clearance} - 19.959)(0.333\text{Max_diameter} - 7.0) \\
 & + (0.027\text{Rotating_speed} - 148.632)(0.333\text{Max_diameter} - 7.0) \\
 & - 569.853
 \end{aligned}$$

3.3 Validation and comparison with empirical model

3.3.1 A test case

Table 3.7 Input and Output of Test Case T1

No	Input Parameters							Observed Parameters		
	DBFF (inch)	Rotating Speed (rpm)	Max Diameter (inch)	Radial Clearance (inch)	Shaft Temperature (°F)	Ambient Temperature (°F)	No. of Bolts	Max Temperature (°F)	Windage Torque (Nm)	Min Pressure (Pa)
T1	25	5400	24	1.5	180	60	20	320.79	- 2.055	- 4345.3

After input the above parameters into regression model, the output temperature is 335.67°F. The prediction expression overestimates the temperature by about 15°F. This is a reasonable prediction.

The regression model is used to predict enclosure temperature after inputting parameters in the given ranges. The temperature values obtained from the regression model can be compared with those calculated from Calistrat’s empirical formula [6].

3.3.2 Comparison with empirical formula

Using Model Fit function in JMP, a regression-based model is constructed and values calculated by this model is obtained. We then proceed to compare these values with results from Calistrat’s empirical formula, since they are both used for the prediction of coupling guard temperature without air-cooling.

In the plots below, temperature values reported in ANSYS CFX are reference value. Calculated values from both empirical formula and regression-based formula are compared with this reference value as shown in Figure 3.11 and Figure 3.12. Note that only calculated temperature values that fall in the range of 100-500 °F are presented below. This is because in practical settings, it is unlikely that enclosure temperature will exceed 500°F. A reference line ($y=x$) is drawn. The closer the points to the line, the better the prediction.

The formula is to be used for temperature prediction in a CFD modeled system, where temperature values obtained from CFD solver are estimated.

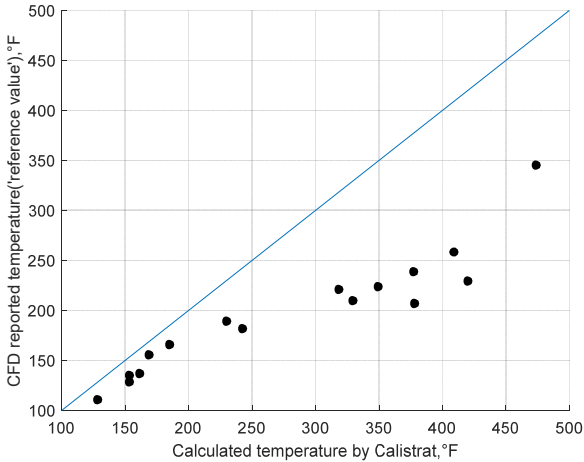


Figure 3.11 Relationship Between Reference Value and Value Calculated by Calistrat's Formula (No. of bolts=36)

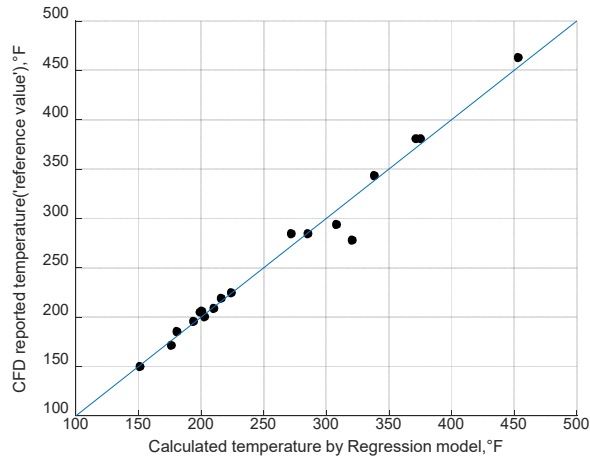


Figure 3.12 Relationship Between Reference Value and Value Calculated by Regression-based Formula (No. of bolts=20, 28, 36)

From the comparison we can learn that;

- 1) Calistrat's formula tends to overestimate enclosure temperature as calculated data points are deviated from the reference line (below $y=x$). The difference of calculated and reference value can be as much as 300°F.
- 2) In Calistrat's formula, number of bolts is not taken into consideration. In the simulation experiments design, number of bolts are set to be 20,28,36 and those bolts locate at maximum diameter on coupling flanges. The heat generated by bolt heads are significant and shall not be neglected.
- 3) The regression-based model can give very accurate prediction of enclosure temperature. This mathematical model considers main effects (single term of each variables) and interaction terms that contain 'Rotating Speed' or

‘Maximum Coupling Diameter’. Because initial simulation shows that above two terms have the most significant effect on enclosure temperature.

The proposed regression model for temperature prediction can be used when input parameter is in ranges listed in Table 3.8.

Table 3.8 Parameter Ranges

Rotating Speed/ rpm	Max Diameter/ inch	DBFF/ inch	Radial Clearance/ inch	Shaft Temperature/ °F	Ambient Temperature/ °C	No. of Bolts
3600 - 7200	18 - 24	20 - 30	1 - 2	120 - 180	60 - 100	12 - 36

4 REGRESSION MODEL FOR GEAR WINDAGE POWER LOSS

4.1 Empirical formula for gear WPL calculation

4.1.1 Prediction expression from AGMA 6011-I03

AGMA 6011-I03 Specifications for High Speed Helical Gear Units includes an equation for windage and churning power loss calculation [29]:

$$P_w' = \frac{d'^2 n^2 b \cos^3 \beta' m_n 1.42 \times 10^{-11}}{A}$$

Where,

P_w' windage power loss per gear, kW

d' operating pitch diameter of gear, mm

n gear speed, rpm

b total face width, mm

β' operating helix angle, °

m_n normal module, mm

A arrangement constant (1000 - 4000, based on arrangement)

In the above empirical formula, geometry variables include pitch diameter d' , face width b , helix angle β' and normal module m_n . Gear speed is also an important variable in the formula, which has a power of 2. Note that arrangement constant has a range of 1000 - 4000, therefore the calculated WPL also falls in a range.

The given formula is used to estimate WPL per gear, therefore the WPL of the gearbox can be calculated by adding up power loss from individual gear.

4.1.2 Prediction expression from Dudley's Gear Handbook

An empirical formula for gear WPL

calculation is proposed in Dudley's Gear Handbook [30]:

$$P_w = 15000 \left(\frac{n}{1000} \right)^3 \left(\frac{D}{2.54} \right)^4 \left(\frac{5L}{2.54} + \frac{D}{2.54} \right)$$

Where,

P_w power loss due to windage, kW

n gear speed, rpm

D diameter of rotating element, m

L length of rotating element, m

The above equation can be divided into two parts. The sides of a gear blank and the periphery of the gear blank before the teeth are cut. Power loss for smooth surfaces on the sides of the gear and pinion:

$$P_{w_side} = 15000 \left(\frac{n}{1000} \right)^3 \left(\frac{D}{2.54} \right)^5$$

Power loss for the periphery of a gear assuming smooth surfaces, such as the gap between helices, etc.:

$$P_{w_periphery} = 15000 \left(\frac{n}{1000} \right)^3 \left(\frac{D}{2.54} \right)^4 \left(\frac{5L}{2.54} \right)$$

The equation will need to be modified to take the gear teeth size and helix angle into consideration. When these factors are considered, a revised equation is proposed:

$$P_m = 15000 \left(\frac{n}{1000} \right)^3 \left(\frac{D}{2.54} \right)^4 \left(\frac{5L}{2.54} \right) \left(\frac{R_f}{\sqrt{\tan \Psi}} \right)$$

where

Ψ helix angle

R_f rough surface adjustment factor, related to diametral pitch

Table 4.1 Relationship Between m_t and R_f

Transverse Diametral Pitch m_t	R_f
4	7.2
6	6.7
10	6.1
16	5.0
24	3.8

From Table 4.1, an approximation can be obtained,

$$R_f = 7.93 - \frac{4.648}{m_t}$$

Below is an example to estimate WPL of a helical gear rotating at 600 rad/s (5729.6rpm), the gear geometry is listed in Table 4.2:

Table 4.2 Helical Gear Geometry

Pitch diameter (mm)	Width (mm)	Module (mm)	Helix angle (°)
288	30	4	15

Power loss for smooth surfaces on the sides of the gear and pinion is then calculated:

$$P_{w_side} = 15000 \left(\frac{n}{1000} \right)^3 \left(\frac{D}{2.54} \right)^5 = 15000 \times \left(\frac{5729.6}{1000} \right)^3 \left(\frac{0.288}{2.54} \right)^5 = 52.876W$$

$$P_L = 15000 \left(\frac{n}{1000} \right)^3 \left(\frac{D}{2.54} \right)^4 \left(\frac{5L}{2.54} \right) \left(\frac{R_f}{\sqrt{\tan \Psi}} \right)$$

$$= 15000 \left(\frac{5729.6}{1000} \right)^3 \left(\frac{0.288}{2.54} \right)^4 \left(\frac{5 \times 0.03}{2.54} \right) \left(\frac{6.8}{\sqrt{\tan 15^\circ}} \right) = 361.776W$$

Total power loss due to windage:

$$P_{w_side} + P_L = 52.876 + 361.776 = 414.652W$$

4.2 Gear WPL calculation using CFD methods

4.2.1 Spur gear simulation in Fluent (2D, steady state)

Before simulation

Gear shrouding has been regarded as an effective way to reduce gear WPL. A parametric study is conducted in ANSYS Fluent in order to study the effect of shroud clearance. Simulation results are compared with experimental data in Lord's paper [31] to validate the computational methods.

Some important assumptions are made:

- 1) Spur gear rotating in pure air and air properties are measured at 25°C;

2) Due to the limitation of 2D simulation, only peripheral WPL can be reported in Fluent. WPL due to gear sides is estimated by an empirical formula,

$$P_{w_side} = 15000 \left(\frac{n}{1000} \right)^3 \left(\frac{D}{2.54} \right)^5$$

3) Peripheral WPL is calculated based on pressure and viscous moment reported in Fluent,

$$P_{w_peripheral} = (T_{pressure} + T_{viscous}) \cdot \omega$$

Total WPL is therefore,

$$P_w = P_{w_side} + P_{w_peripheral}$$

4) Only two gear teeth are modeled, and periodic boundary conditions are employed in order to save computing costs;

5) In Lord's experiment, an axial clearance of 1mm is maintained. But in our 2D simulation, no axial clearance is considered.

Simulation procedures

A 2D drawing of gear teeth is imported to ICEM where structured mesh is generated. Simulation is then conducted in Fluent after boundary conditions are properly defined. A description of boundary conditions can be found in Figure 1.4.

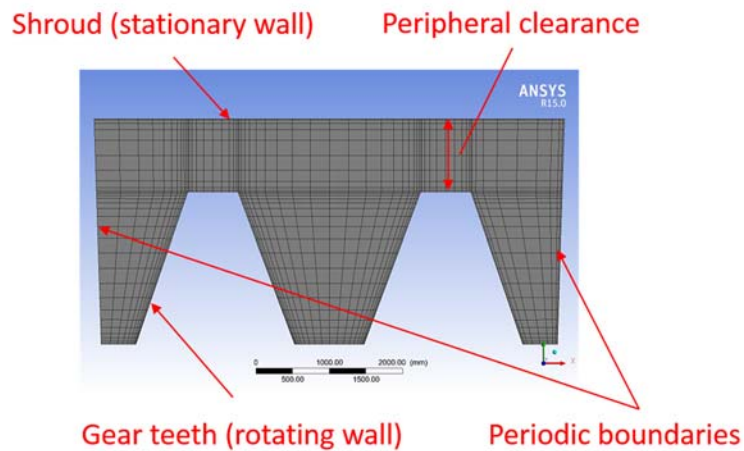


Figure 4.1 Boundary Conditions in Fluent

Simulation results are compared with Lord's experimental data [31] since his experiment to measure spur gear windage power is detailed and comprehensive. Geometries in CFD simulation are therefore chosen to be the same as these in Lord's experiments, as listed in Table 4.3.

Table 4.3 Spur Gear Geometry for 2D Simulation

Module (mm)	Pitch diameter (mm)	Pressure angle (°)	Face width (mm)
1	200	20	40

Shroud clearance is defined as the distance between gear tip to shroud.

Experimental data is available for 1, 5 and 10mm shroud clearance, therefore CFD simulation starts with these parameters.

A rotating reference frame is introduced and boundary conditions set as below:

- 1) Gear teeth (rotating wall);
- 2) Shroud (counter-rotating wall);
- 3) Periodic boundaries.

Results

Convergence is reached when both the residuals of the equations fall below 10^{-4} and monitored torque value keeps constant magnitude. Figure 4.2 shows pressure contour and velocity streamline obtained in CFD-POST.

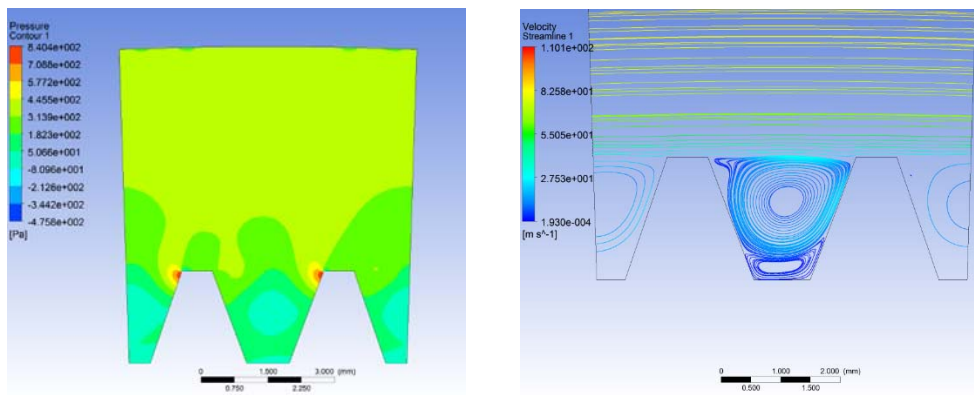


Figure 4.2 Pressure Contour and Velocity Streamline for 2D Spur Gear

After simulation results are compared with experimental data, more simulations can be carried out to develop a generic understanding of the effect of shroud clearance.

A mesh independence study is also conducted to ensure that simulation results are not affected by mesh size, especially that in the near wall region. After initial simulations, appropriate mesh size can be determined for each shroud clearance.

Different configurations are modeled in Fluent. After a steady state is reached, WPL for each configuration is obtained and plotted in Figure 4.3. Experiments with the same configurations were conducted by Lord and data recorded in Figure 4.4. These two figures are used for initial comparison of experimental and simulation results.

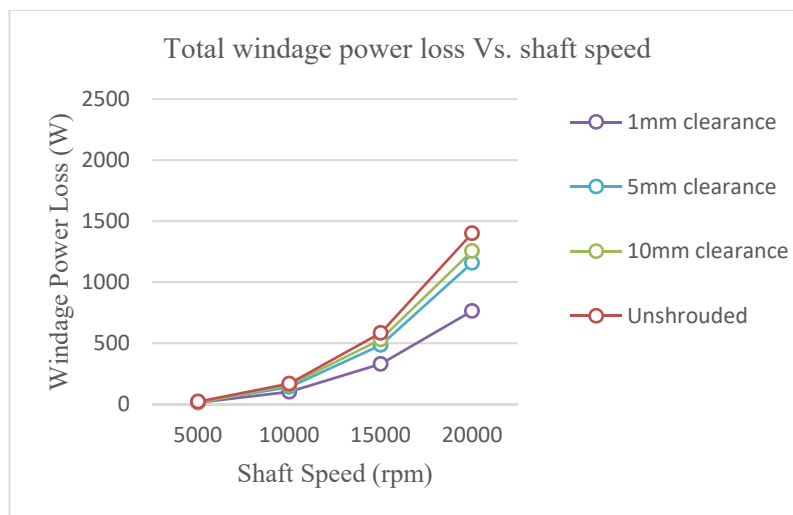


Figure 4.3 Simulation Results Summary

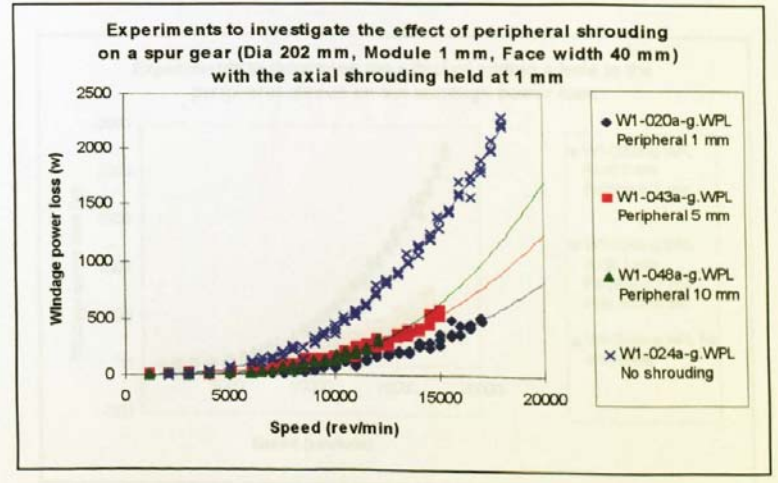


Figure 4.4 Experimental Data from Lord’s Paper (Reprinted from [31])

From the simulation results in Figure 4.3, we find that WPL increases as rotating speed increases. When there is no shrouding, the largest WPL is observed. At same rotating speed, as radial clearance decreases, WPL also decreases. The observation justifies the effectiveness of shroud in reducing WPL. A shroud clearance of 1mm appears to have the best anti-windage effect. When comparing 5mm and 10mm shroud clearance, a slightly larger WPL reduction is noticed with 5mm clearance.

Compared with experimental data in Figure 4.4, the trend of WPL is well reproduced by simulation. Simulation results underestimate the power loss when the gear is unshrouded. This can be explained due to the limitations of 2D simulation:

- 1) In 2D simulation, only peripheral WPL can be reported from Fluent, the WPL of gear side is calculated based on empirical formula. Therefore, the accuracy of the overall prediction can be affected by the empirical formula.

2) There is an 1mm axial shroud clearance in the experiments. However, in 2D simulations it is assumed that gear has infinite width. The effect of the axial shroud is not taken into consideration during the simulation.

Figure 4.5 shows a one-on-one comparison of CFD results and experimental results at different rotating speeds and shroud clearances. Experimental data is not available for several configurations and a shroud clearance of 30mm is regarded as ‘unshrouded’ in the simulation.

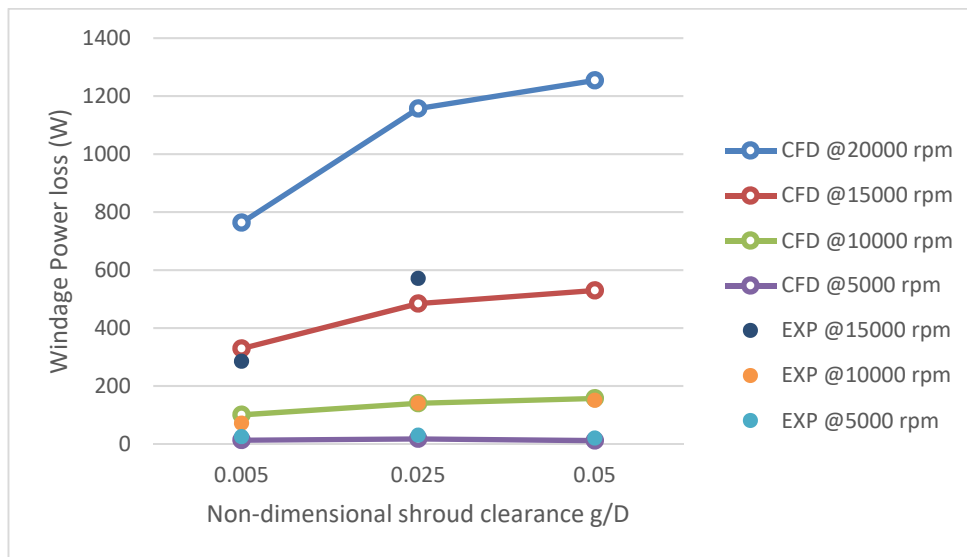


Figure 4.5 WPL vs. Non-dimensional Shroud Clearance

Besides the trend observed in previous plots, it can be found from Figure 4.6 that as shroud clearance keep increasing, its effect on WPL reduction become less obvious.

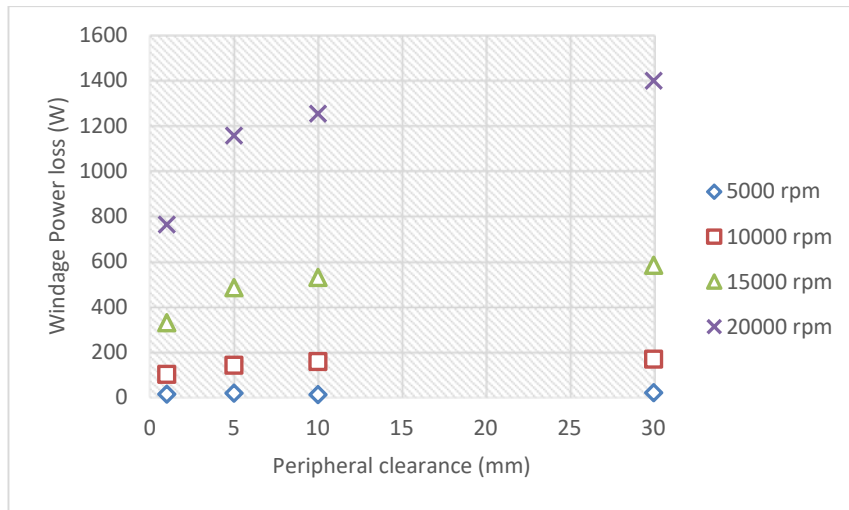


Figure 4.6 WPL vs. Peripheral Clearance

4.2.2 Spur gear simulation in CFX (3D, steady state)

Geometry and meshing

Two full-scale gear teeth are modeled and steady state simulation is conducted in CFX. Gear characteristic is listed in Table 4.4 and structured mesh generated as shown in Figure 4.7.

Table 4.4 Spur Gear Geometry for 3D Simulation

Pitch diameter (mm)	Width (mm)	Module (mm)	Tip diameter (mm)	Pressure Angle (°)
288	30	4	296	20

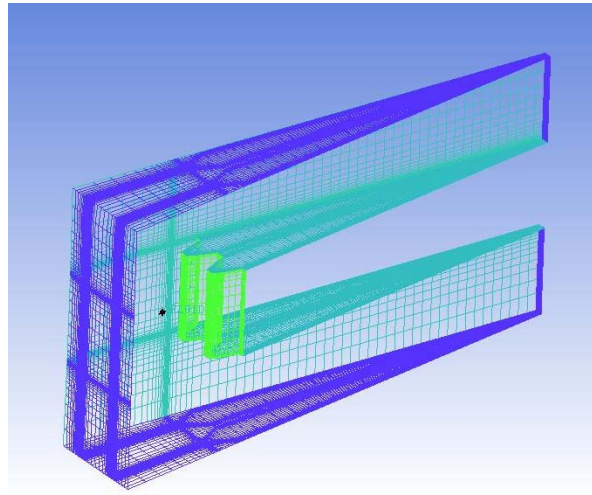


Figure 4.7 Structured Mesh for Two Spur Gear Teeth

Boundary conditions in CFX

Some assumptions are made:

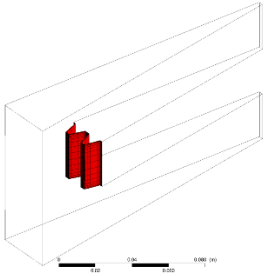
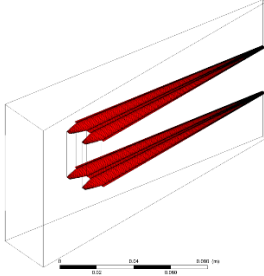
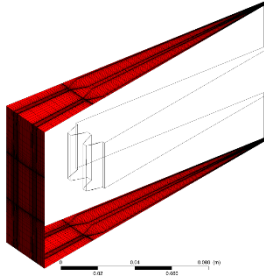
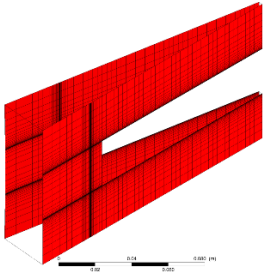
1) The spur gear is rotating in pure air with physical properties evaluated at 25°C
($\rho = 1.185 \text{ kg / m}^3$, $\mu = 1.831 \times 10^{-5} \text{ Pa} \cdot \text{s}$)

2) A 10° section with periodic boundary condition can be used for simulation instead of whole model

A rotating reference frame is used in the simulation, so that moving mesh is avoided. In CFX, fluid domain is set to rotate at constant speed. Steady state simulation is conducted and convergence is determined when monitored torque value remain unchanged and residuals are sufficient low (Smaller than 10^{-4})

Detailed boundary conditions are listed below:

Table 4.5 Boundary Conditions for 3D Gear Simulation

Location	Name	Description
	gear	<p>Type: Wall</p> <p>Gear teeth region, torque on this region can be reported in CFD-POST, used to calculate WPL.</p>
	gear_side	<p>Type: Wall</p> <p>Side of gear, torque on this region can be reported in CFD-POST, used to calculate WPL.</p>
	opening	<p>Type: Opening</p> <p>Opening boundary condition allows air to go in or out of the domain. This is to simulate that gear is unshrouded.</p>
	periodic_1, periodic_2	<p>Type: Interface (periodic boundary)</p> <p>Periodic boundary condition imposed so that only two gear teeth need to be modeled.</p>

Results

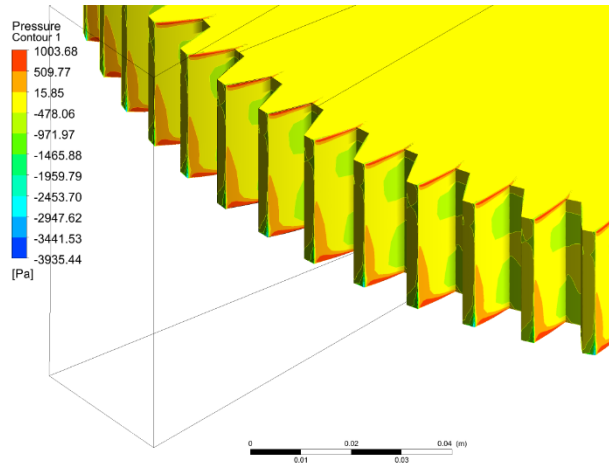


Figure 4.8 Pressure Contour of Gear Teeth @ 400 rad/s

From the pressure contour in Figure 4.8, peak pressure is observed at areas where the teeth flank intersects with side of the gear. The contour profile is almost symmetry about gear mid-plane. This can be explained that gear geometry is symmetry about the plane and the pressure contour is expected to be symmetry as well.

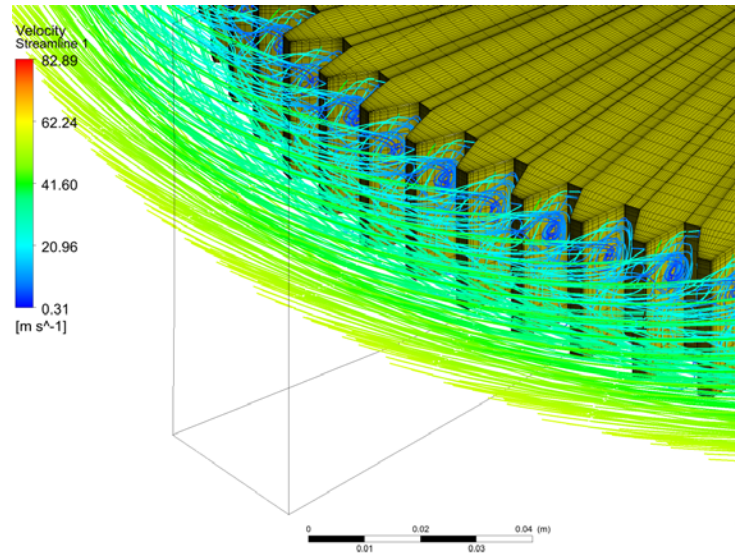


Figure 4.9 Velocity Streamline @ 400 rad/s (Velocity Relative to Rotating Domain)

The velocity streamlines in Figure 4.9 are plotted relatively to the rotating domain. Therefore, velocity at gear teeth region is smaller compare to other regions in the domain. When fluid interact with gear teeth, it discharges across the flank and exit the gap between gear teeth from the two ends.

With torque value reported in CFD-POST, WPL can be calculated by multiplying torque by angular velocity. A good agreement with experimental results from [20] is obtained as shown in Figure 4.10 and this validates the CFD model and boundary conditions setup in CFX.

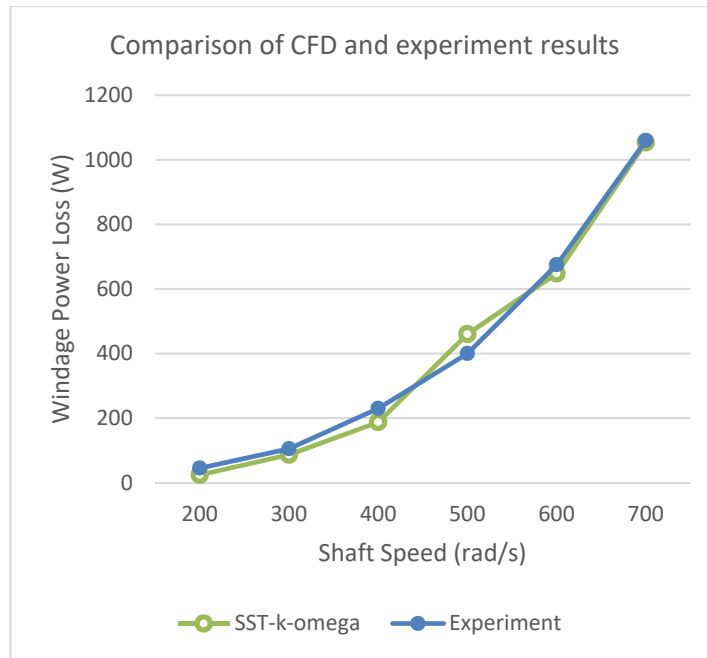


Figure 4.10 Comparison of CFD and Experiment Results for 3D Spur Gear Model

4.2.3 Helical gear simulation in CFX (3D, steady state)

Geometry and meshing

Geometry characteristic of the helical gear is the same as in Table 4.2. Similar boundary conditions are used for helical gear simulation. Periodic boundary conditions enable that using two gear teeth, instead of whole gear for simulation. Figure 4.11 shows that simulation domain is a 10° sector derived from whole geometry.

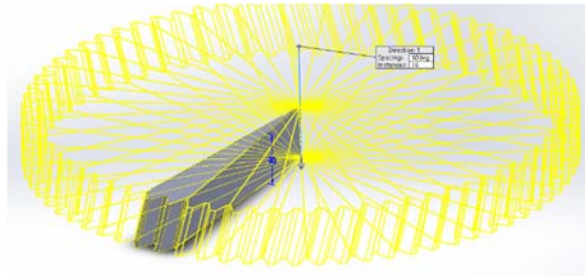


Figure 4.11 Simulation Domain Derived From Whole Gear

Structured mesh is generated for the helical gear in ANSYS ICEM (Figure 4.12)

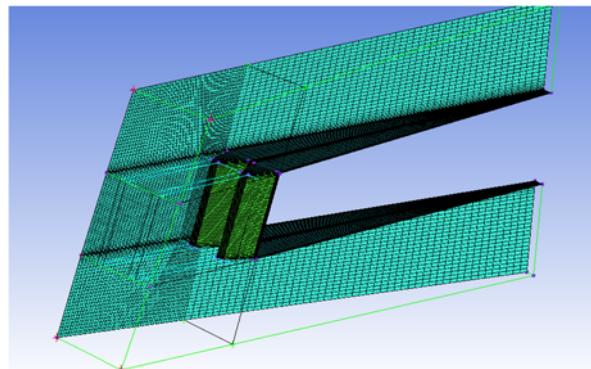


Figure 4.12 Structured Mesh of Helical Gear Teeth

Boundary condition in CFX

Similar boundary conditions used by 3D spur gear is used for helical gear.

Results

After steady state is reached, that is when monitored torque value maintains constant and residual is sufficient small (Smaller than 10^{-4}). Pressure contour and velocity vector is plotted in CFD-POST.

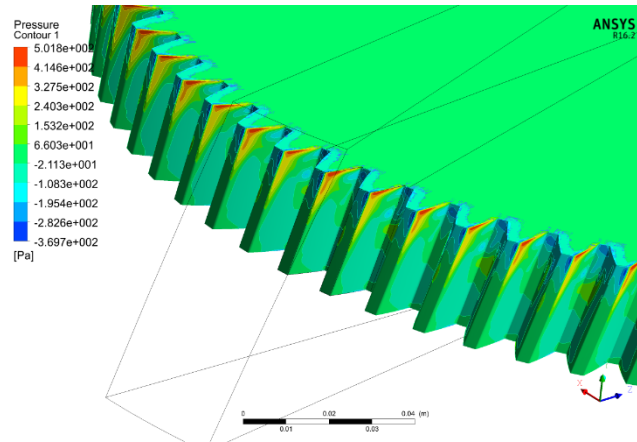


Figure 4.13 Pressure Contour of Helical Gear Teeth @ 200 rad/s

From Figure 4.13, concentration of pressure is seen at one side of the gear teeth as opposed to the observation in spur gear case. This is because that helical gear is not symmetry about its mid plane. When rotating in the air, one side of the gear encounter the fluid flow earlier than the other side and direct impact on the gear teeth results in pressure concentration.

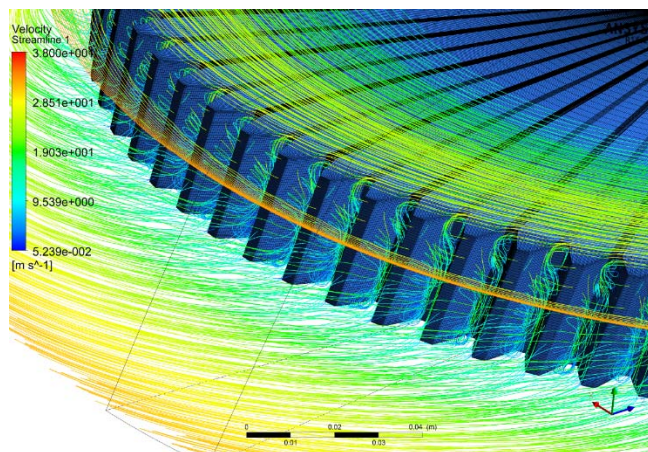


Figure 4.14 Velocity Streamline of Helical Gear @ 200rad/s

From Figure 4.14, fluid is drawn from one side of the gear teeth, after revolution expelled from the other side. In the helical gear case, the fluid first interact with one side of the gear teeth and the direct impact on this side causes the pressure concentration as discussed above.

Numerical predictions are compared with experimental data from [32], as shown in Figure 4.15. A good agreement is obtained and this further validates that CFD model can give accurate prediction for WPL.

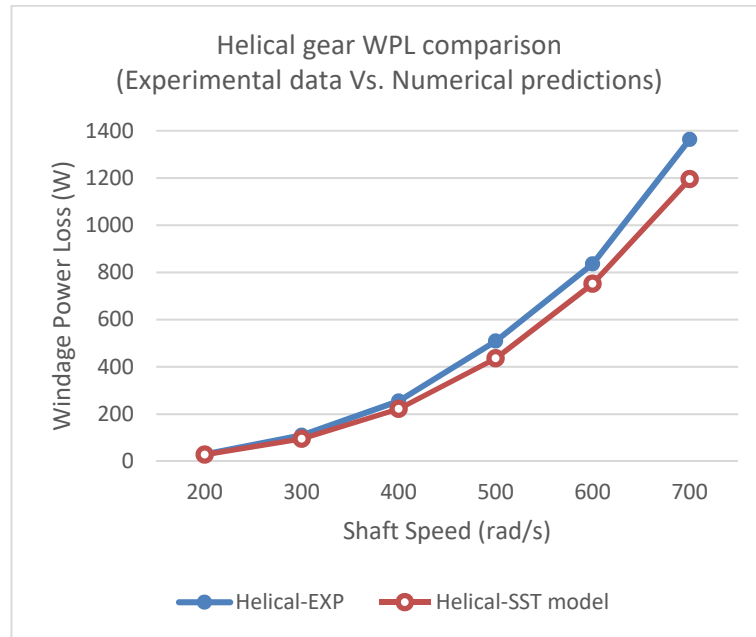


Figure 4.15 Helical Gear WPL Comparison

4.3 Gear windage power loss regression model

4.3.1 Parameter choice and design of experiments

The parameters are chosen so that facilitate comparison with available experimental data, practical factors are also taken into consideration when choosing the parameter ranges. For example, typical tooth size in high power turbo gears (For which WPL is considered an issue) starts at a minimum module of 2 mm, but are more common in the range from 3 to 8 mm.

WPL shall not be neglected when the tip speed is above 10000 ft/min (50.8 m/s), therefore tip speed is calculated for each parameter combination to ensure that a significant enough tip speed is reached.

The parameters are chosen as below and ranges listed in Table 4.6:

Table 4.6 Parameters and Their Ranges

Parameter	Range
Pitch diameter/ mm	144 – 288
Tooth width/ mm	20 – 60
Normal module/ mm	4 – 8
Helix angle/ °	0 – 30
Rotating speed/ rpm	4000 – 8000

Design of Experiment (DOE) features of JMP software are utilized. Simulation experiments are carried out according to a central composite design based on response

surface technology (RSM) [33]. A more detailed description about the software and its DOE feature is included in the appendix.

Table 4.7 Design of Experiments and Simulation Results

No. simulation	Input parameters					Observed parameters
	Pitch Diameter/ mm	Tooth width/ mm	Normal module/ mm	Helix angle/ °	Rotating speed/rpm	Windage power loss/ W
1	144	20	4	0	4000	19.60
2	144	20	4	30	8000	318.14
3	144	20	8	0	8000	405.64
4	144	20	8	30	4000	46.91
5	144	40	6	15	6000	113.80
6	144	60	4	0	8000	174.92
7	144	60	4	30	4000	28.57
8	144	60	8	0	4000	96.51
9	144	60	8	30	8000	422.23
10	216	20	6	15	6000	659.73
11	216	40	4	15	6000	135.59
12	216	40	6	0	6000	441.08
13	216	40	6	15	4000	170.06
14	216	40	6	15	6000	250.70
15	216	40	6	15	6000	1051.18
16	216	40	6	15	8000	1401.57
17	216	40	6	30	6000	1334.23
18	216	60	8	15	6000	747.14
19	216	60	6	15	6000	608.06
20	288	20	4	0	8000	1354.15
21	288	20	4	30	4000	466.17
22	288	20	8	0	4000	559.45
23	288	20	8	30	8000	2510.05
24	288	40	6	15	6000	1611.32
25	288	60	4	0	4000	505.17
26	288	60	4	30	8000	2882.73
27	288	60	8	0	8000	4852.03
28	288	60	8	30	4000	158.42

4.3.2 Multivariable regression formulas for gear WPL

The mathematical relationship between response and several related parameters are fitted using second order polynomial. A general second order polynomial mathematical model can be described as follows [34]:

$$Y = b_0 + \sum_{i=1}^k b_i X_i + \sum_{i=1}^k b_{ii} X_i^2 + \sum_{j>i}^k b_{ij} X_i X_j$$

Coefficient b_0 is intercept term, b_i are linear terms, b_{ii} are quadratic terms, b_{ij} are interaction terms.

These coefficients can be estimated using least square technique and the values can be reported in JMP. Some coefficients are omitted as they are not significant according to Student's t-test [35] and removed by backwards elimination. Statistical significant parameters include:

Pitch Diameter, Rotating speed, Normal module, Tooth width (Main effect)

Pitch diameter • Rotating speed, Normal module • Helix angle, Tooth width • Rotating speed, Normal module • Rotating speed, Pitch diameter • Tooth width, Tooth width • Helix angle (Interactions)

Prediction formula is generated in JMP and MATLAB code is written accordingly. The final form of the expression is (Units of parameters in the expression is the same as those in Table 4.7):

$$\begin{aligned}
\text{WPL} = & 108.704\text{Normal_module} + 10.241\text{Pitch_D} + 0.340\text{Rotating_speed} \\
& + 9.413\text{Tooth_W} + (0.0005\text{Rotating_speed} - 3.0)(7.621\text{Pitch_D} \\
& - 1646.324) + (0.0005\text{Rotating_speed} - 3.0)(12.648\text{Tooth_W} \\
& - 505.925) - 1.0(18.407\text{Helix_angle} \\
& - 276.110)(0.5\text{Normal_module} - 3.0) + (0.05\text{Tooth_W} \\
& - 2.0)(3.104\text{Pitch_D} - 670.609) + (0.0005\text{Rotating_speed} \\
& - 3.0)(113.069\text{Normal_module} - 678.415) - 1.0(0.05\text{Tooth_W} \\
& - 2.0)(13.079\text{Helix_angle} - 196.194) - 4453.001
\end{aligned}$$

4.3.3 Regression model validation and comparison

In order to validate the accuracy of the regression based model, WPL is calculated using regression model and compared with that from CFD simulation. A plot with a reference line ($y=x$) is used to illustrate the accuracy (Figure 4.16). For the same input parameter set, WPL is obtained from both regression model (x) and CFD simulation (y). If point (x,y) falls on the reference line ($y=x$), it means that prediction based on regression model is the same as CFD results (Reference value). The closer the points to the $y=x$, the more accurate the regression model.

$R^2 = 92.94\%$ for the regression model.

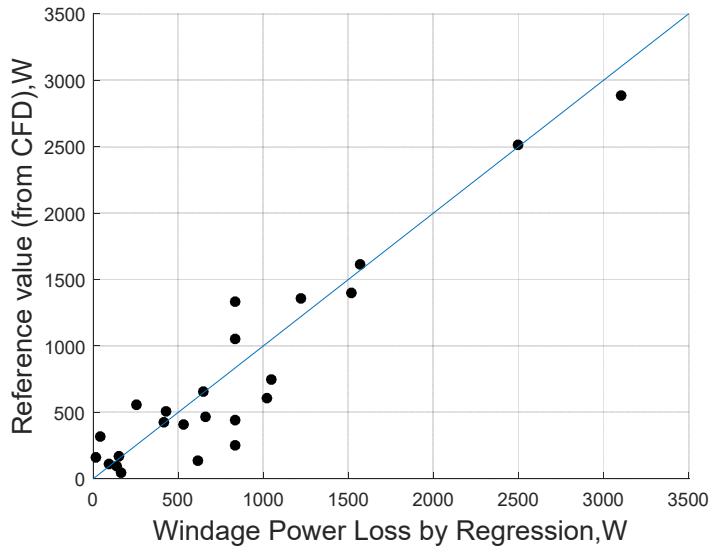


Figure 4.16 Relationship Between Reference Value and Value Calculated by Regression-based Formula

Recall the empirical formula presented in AGMA6011-I03, WPL is calculated using the formula with same set of parameter in design of experiment, comparative results are plotted in Figure 4.17.

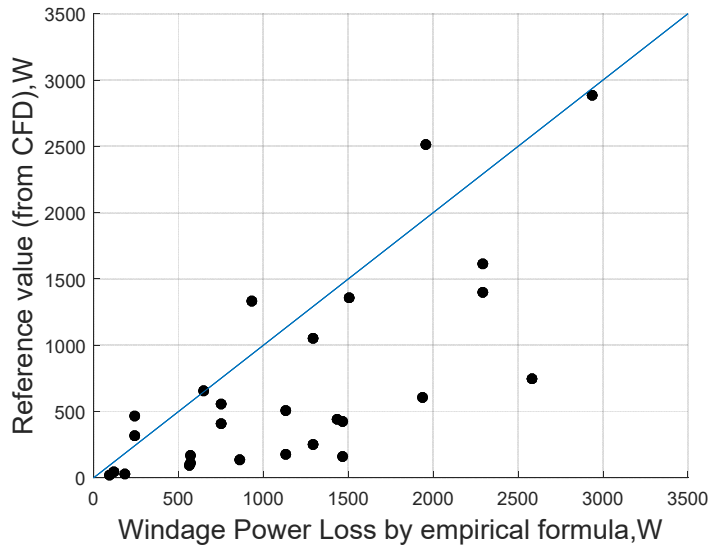


Figure 4.17 Relationship Between Reference Value and Value Calculated by Empirical Formula

$$RR^2 = 57.83\%^2 = 57.83\% \text{ for empirical formula.}$$

A test case where data calculated from regression model is compared with experimental data. The gear geometry in the test case is listed in Table 4.8. The speed of the shaft ranges from 500 rad/s to 700 rad/s.

Table 4.8 Gear Geometry for Test Case

Pitch diameter (mm)	Width (mm)	Module (mm)	Helix angle (°)
288	30	4	15

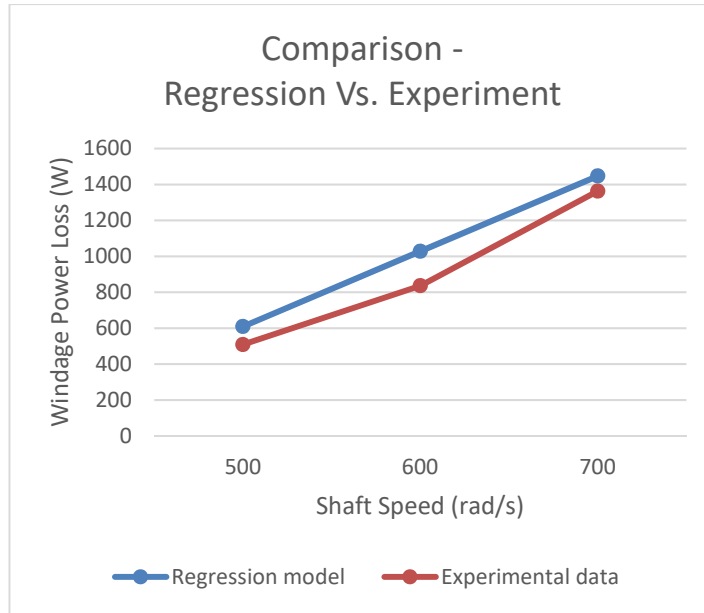


Figure 4.18 Comparison Between Regression and Experimental Results

From Figure 4.18, the error at 500 rad/s, 600 rad/s, 700 rad/s can be calculated and they are 19.64%, 22.97% and 6% respectively.

The above comparison cases use the same geometry. Three simulation test cases with different geometry and rotating speeds are also designed to further validate the correlation.

Table 4.9 Parameters in Test Cases

No. simulation	Input parameters					Observed parameters
	Pitch Diameter/ mm	Tooth width/ mm	Normal module/ mm	Helix angle/ °	Rotating speed/rpm	Windage power loss/ W
T1	180	50	4	15	7639	457.39
T2	200	40	6	30	6684	694.21
T3	252	30	8	15	5729	1372.36

Calculated value using regression model are: 537.31W, 860.61W, 1126.08W.

The errors are 17.5%, 23.97%, 21.87%. The regression model tends to overpredict the WPL. The test data points are also plotted in red for reference (Figure 4.19).

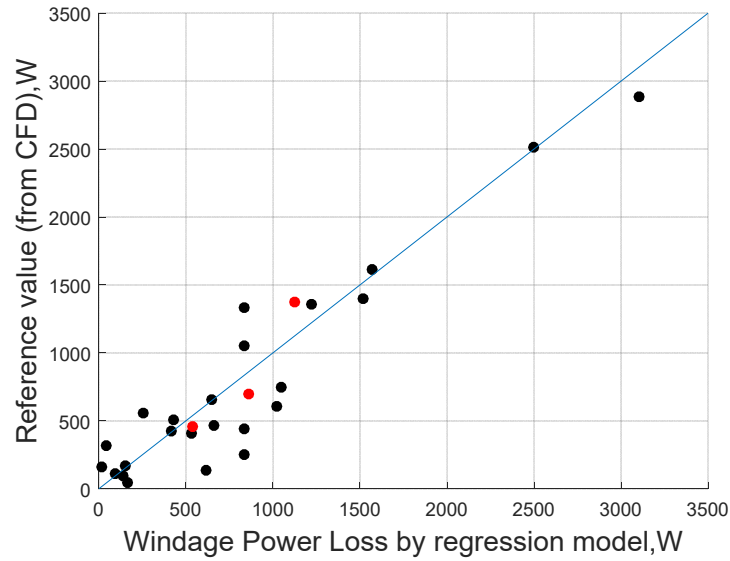


Figure 4.19 Test Cases Points Plotted in Red

4.4 Two meshing spur gears simulation in Fluent (3D, transient)

4.4.1 Simulation description

We have discussed steady state simulation of WPL for individual spur/helical gear rotating in air. When consider two meshing gears, squeezing due to gear engagement has to be taken into consideration. Squeezing power loss, together with windage/churning power loss are called hydraulic power loss.

Compared with previous simulation, there are several changes in transient simulation, therefore a tutorial is written (See Appendix A) to guide reader through the simulation process.

A gear set immersed in oil is tested and geometry of the gear set is reported [24]. The gearbox is filled with oil ($\rho = 824.5 \text{ kg / m}^3$, $\mu = 0.05463 \text{ Pa} \cdot \text{s}$). Three different rotating speed is simulated, 2000 rpm (209.44 rad/s), 5000rpm (523.6 rad/s), 6000rpm (628.3 rad/s). Gear geometry used in experiments is listed in Table 4.10:

Table 4.10 Gear Geometry for Meshing Gear Simulation

No. of gear teeth	Module/mm	Pressure angle/°	Gear width/mm
23	4	20	40

4.4.2 Meshing and boundary condition setup in Fluent

A gearbox composed of two identical gears are modeled. Symmetry boundary conditions are used so that only half of the gearbox geometry is modeled as shown in Figure 4.20, by doing so computational time is saved.

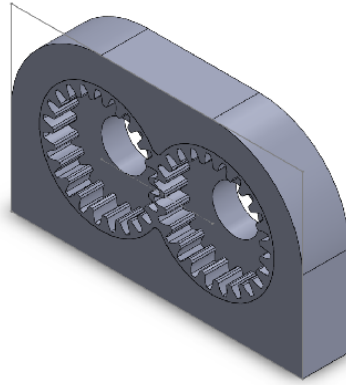


Figure 4.20 Numerical Model of Gearbox (Half of Gearbox Geometry)

A detailed tutorial is written (See Appendix A) to demonstrate the simulation process, including meshing and boundary setups in Fluent.

4.4.3 Post processing

Post processing can be done in CFD-Post, where velocity contour, pressure contour at different time can be plotted. We can also create expression to evaluate quantitative data from flow results. The expressions can be used to create XY plots and creating tables.

1) Velocity contours are plotted as shown in Figure 4.21 and Figure 4.22

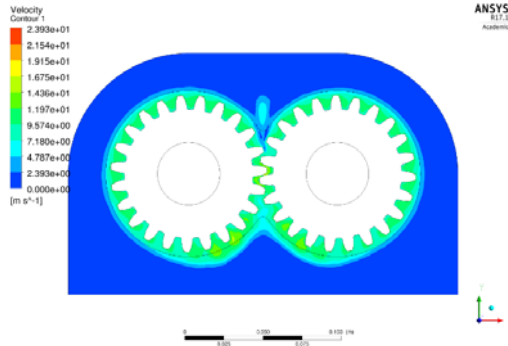


Figure 4.21 Velocity Contour at 0.01s of Flow Time

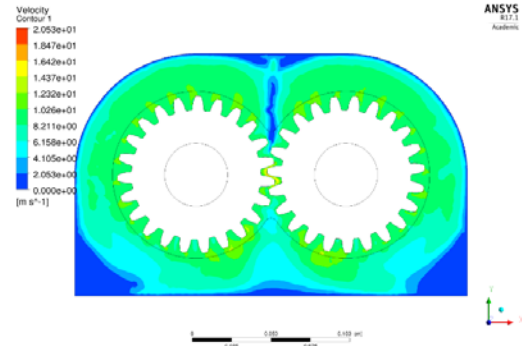


Figure 4.22 Velocity Contour at 0.025s of Flow Time

2) Pressure contours are plotted as shown in Figure 4.23 and Figure 4.24

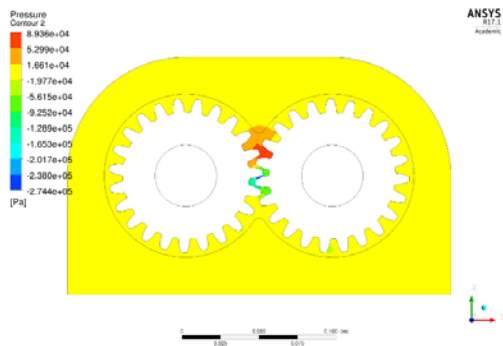


Figure 4.23 Pressure Contour at 0.01s of Flow Time

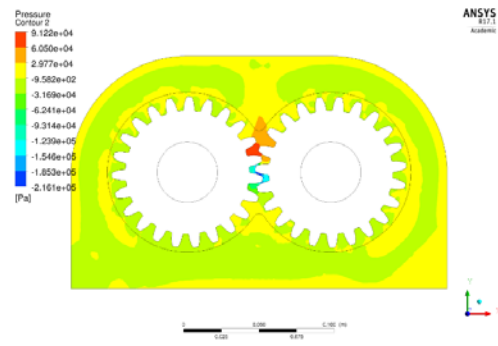


Figure 4.24 Pressure Contour at 0.025s of Flow Time

3) Evolution of torque for Gear 1 & Gear 2

The hydraulic loss (Windage/churning + squeezing) can be calculated by multiplying the torque on gear teeth with rotating speed.

The charts in Figure 4.25 show the evolution of torque as rotating degree increases. Even though the value fluctuates a lot at the beginning, it stabilizes as time goes. The averaged torque can be estimated from available data points.

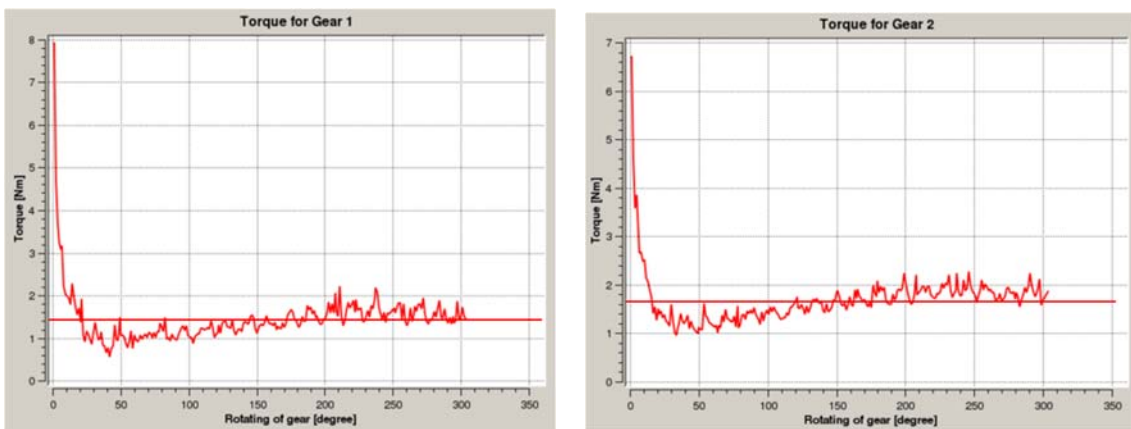


Figure 4.25 Evolution of Torque on Gear Teeth 1 & 2 @2000rpm

4) Evolution of churning power loss for Gear 1 & Gear 2 is plotted in Figure 4.26.

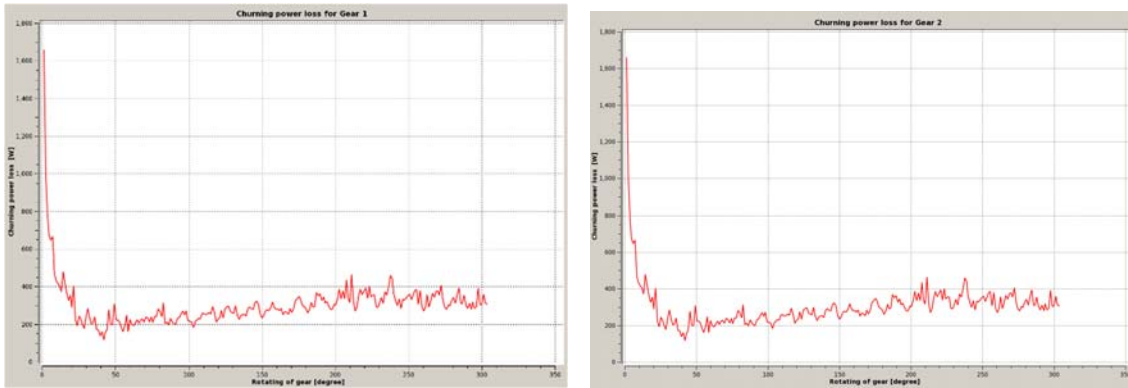


Figure 4.26 Evolution of Power Loss on Gear Teeth 1 & 2 @2000rpm

The evolution of torque on gear teeth 1 & 2 when rotating at 5000rpm and 6000 rpm is also plotted in Figure 4.27 and Figure 4.28, the hydraulic torque can be read from the plot.

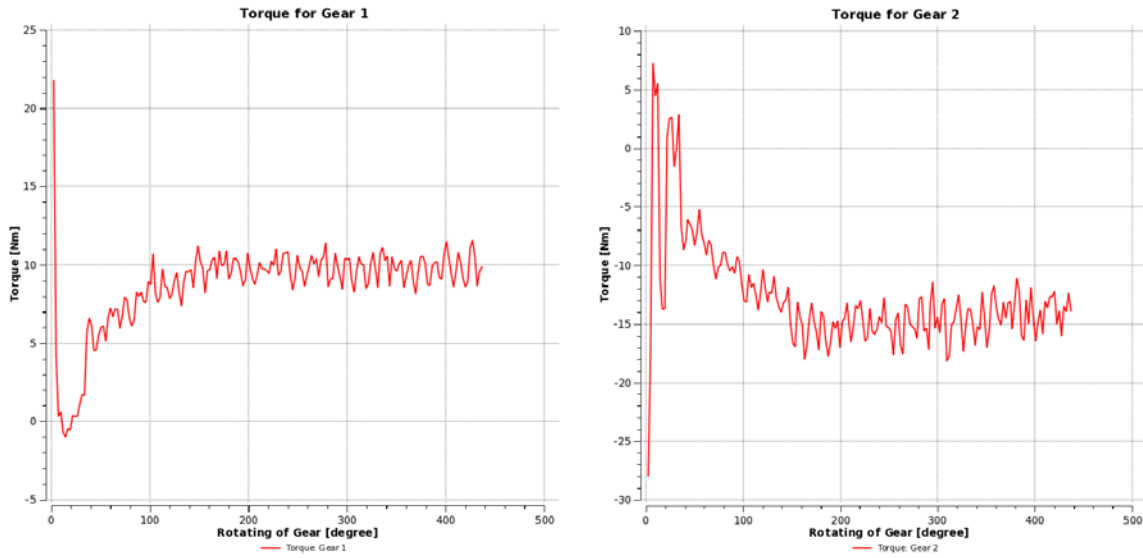


Figure 4.27 Evolution of Torque on Gear Teeth 1 & 2 @5000rpm

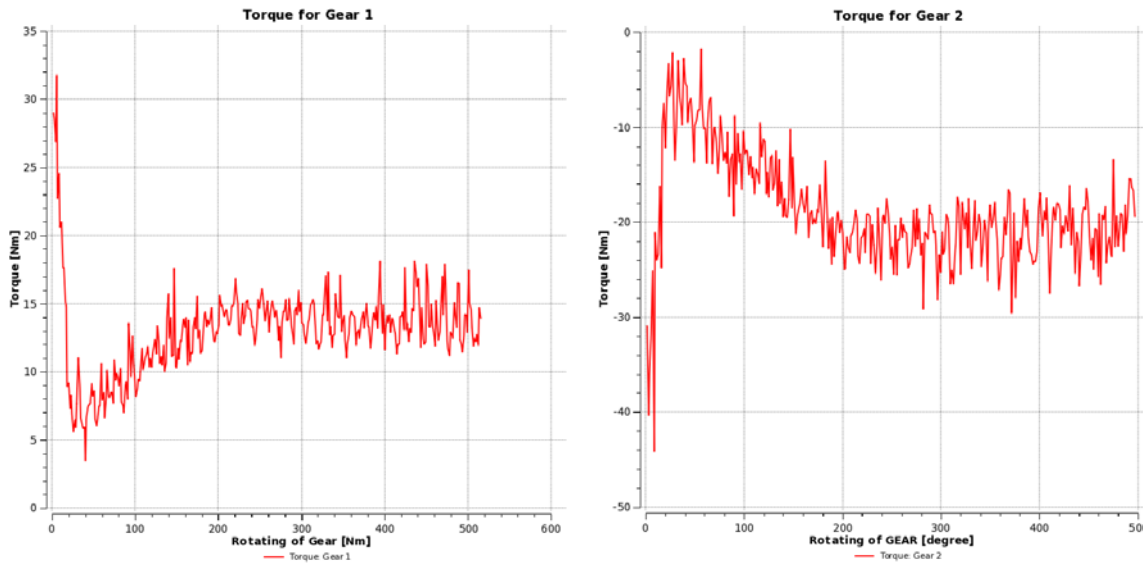


Figure 4.28 Evolution of Torque on Gear Teeth 1 & 2 @6000rpm

4.4.4 Comparison & discussion

The geometry of the gear set used for experiment is not described in details, the numerical model is built to match as much as possible (Number of gear teeth, module, gear width). The tip diameter in the numerical is 100 mm, in experiments the tip diameters are 96.5mm and 102.5mm. Even though this is not a one-on-one comparison, it is still of interest to see how simulation data points will be placed on the plot. From the experiments plot provided, it can be found that as tip diameter increases hydraulic torque also increases. It is expected that simulation data points to fall in between the two experimental data point.

An average churning power loss for the gearbox is estimated from the transient simulation plot. Since a symmetry boundary condition is used, the actual power loss for gearbox can be obtained by doubling the simulation results. For instance, when the rotating speed is 5000rpm, for gear 1 the torque is 9 Nm, gear 2 the torque is -14 Nm. The total torque on gear teeth can then be calculated: (Absolute value of torque)

$$(9 + 15) \times 2 = 48Nm$$

For another case where rotating speed is 6000rpm, similar method is used to obtain the calculated torque on gear teeth. The torque can be read from chart and total torque:

$$(14 + 24) \times 2 = 76 Nm$$

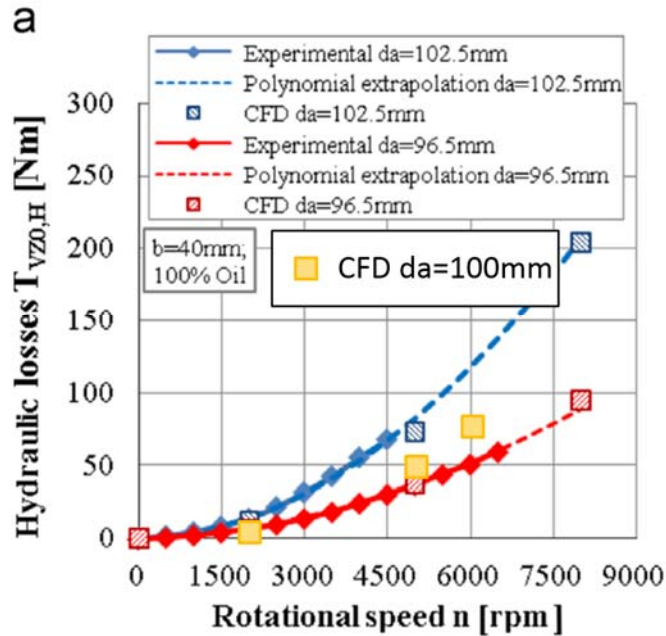


Figure 4.29 Experimental Results from Literature for Comparison (Adapted from [24])

From Figure 4.29, simulation data points (CFD da=100mm) is overlaid onto the plot from the literature. Also, it can be found that CFD data of da=100mm is in between experimental da = 96.5mm and 102.5mm. This confirms previous arguments and proves that simulation results are reasonable.

5 CONCLUSION AND FUTURE WORK

5.1 Conclusion

The simulation of coupling guard temperature and Gearbox Windage Power Loss was conducted in ANSYS CFX and Fluent. Both 2D and 3D simulation results were compared with experimental results from the literature. Good agreement was obtained between simulation and experimental results, which confirmed the predictability of WPL using CFD software. The Multivariable Regression Formulas (MRF) were then developed based on simulation results. Design of Experiment (DOE) was utilized to minimize simulation runs, and extensive simulation was conducted to obtain data for the development of MRF. The accuracy of the MRF was validated by several test cases. A case study regrading coupling guard temperature was also performed in collaboration with industry partners to address practical problems.

The conclusions from the research are:

- 1) CFD software, i.e. ANSYS FLUENT/ CFX have the capacity to predict the temperature on couplings guards and gear or gear sets WPL;
- 2) The Windage flange on coupling guard fails to reduce temperature on coupling guard. Guard temperature drops with increased radial clearance;
- 3) Decrease peripheral shroud clearance of gear lowers gear WPL;

- 4) MRF gives accurate prediction of coupling guard temperature and gear WPL, they are also accurate for input parameter sets that were not used to obtain MRF;
- 5) Sets of input parameters selected through Design of Experiments saved computation cost, i.e. use minimal number of parameter sets.

5.2 Future work

Current WPL prediction focus on individual gear rotating in air. Future work includes expanding current MRF parameters and their ranges for further applications, developing MRF for the meshing gear sets and identifying factors that influence the gearbox WPL. Following is proposed for future work:

- 1) Refine CFD model used in the case study as more physical testing results become available and consider radiation effect in the simulation;
- 2) Include other geometry parameters in coupling guard temperature regression model and conduct test cases to further validate the model;
- 3) Obtain mesh independent results for minimum pressure and develop prediction expression;
- 4) Identify key influencing factors of gearbox WPL;
- 5) Conduct parametric studies of factors that influence gearbox WPL and provide guidelines on reducing WPL.

REFERENCES

- [1] T. Weiss and M. Hirt, "Efficiency Improvements for High Speed Gears of the 100 MW Class," *VDI Berichte*, vol. 1665, pp. 1161-1174, 2002.
- [2] C. N. Eastwick and G. Johnson, "Gear Windage: A review," *Journal of Mechanical Design*, vol. 130, p. 034001, Mar 2008.
- [3] Y. Z. Ge, X. M. Lei, Y. C. Zhang, and P. Liu, "Influence Factors and Calculating Methods for Gear Windage Power Loss," in *Applied Mechanics and Materials*, pp. 602-605, 2011.
- [4] Altra Industrial Motion Corp. (10/2016). *Ameridisc High Performance Disc Couplings*. Available: <http://www.ameridrives.com/products/disc-couplings/ameridisc-disc-couplings>
- [5] American Petroleum Institute, "Special Purpose Couplings for Petroleum, Chemical and Gas Industry Services," ed. Washington DC: American Petroleum Institute, p. 45, 2007.
- [6] M. M. Calistrat and R. Munyon, "Design of Coupling Enclosures," in *Proceedings of the Fourteenth Turbomachinery Symposium*, pp. 51-57, 1985.
- [7] M. M. Calistrat, "Recent Case Histories with Coupling Enclosures," in *Proceedings of Nineteenth Turbomachinery Symposium*, pp. 37-42, 1990.
- [8] J. R. Mancuso, *Couplings and Joints: Design, Selection & Application*. New York: CRC Press, 1999.
- [9] D. Carter, M. Garvey, and J. P. Corcoran, "The Baffling and Temperature Prediction of Coupling Enclosures," in *Proceedings of the Twenty-Third Turbomachinery Symposium*, pp. 115-123, 1994.
- [10] S. Pennington and K.-D. Meck, "Effectiveness of Windage Features on High Speed Couplings," in *Proceedings of the Forty-First Turbomachinery Symposium*, Houston, Texas, 2012.
- [11] A. Thompson, T. Zhai, A. Palazzolo, and A. Keshmiri, "Coupling Guard Temperature and Windag Power Loss: CFD Analysis and Experiments," in *Proceedings of the Forty-fifth Turbomachinery Symposium*, Houston, Texas, 2016.

- [12] V. Jariwala, J. Hardin, and D. Turner, "Computational Investigation of Coupling Guard Heating and Mitigation," in *Proceedings of the Forty-Third Turbomachinery Symposium*, Houston, Texas, 2014.
- [13] P. Dawson, "Windage loss in larger high-speed gears," *Proceedings of the Institution of Mechanical Engineers, Part A: Journal of Power and Energy*, vol. 198, pp. 51-59, 1984.
- [14] Y. Diab, F. Ville, P. Velex, and C. Changenet, "Windage Losses in High Speed Gears - Preliminary Experimental and Theoretical Results," *Journal of Mechanical Design*, vol. 126, pp. 903-908, 2004.
- [15] Y. Diab, F. Ville, and P. Velex, "Investigations on Power Losses in High-speed Gears," *Proceedings of the Institution of Mechanical Engineers Part J-Journal of Engineering Tribology*, vol. 220, pp. 191-198, 2006.
- [16] F. Chaari, M. B. Romdhane, W. Baccar, T. Fakhfakh, and M. Haddar, "Windage Power Loss in Spur Gear Sets," *Wseas Transactions on Applied and Theoretical Mechanics*, pp. 159-168, 2012.
- [17] K. Al-Shibl, K. Simmons, and C. N. Eastwick, "Modelling Windage Power Loss from an Enclosed Spur Gear," *Proceedings of the Institution of Mechanical Engineers Part a-Journal of Power and Energy*, vol. 221, pp. 331-341, 2007.
- [18] S. Pallas, Y. Marchesse, C. Changenet, F. Ville, and P. Velex, "A Windage Power Loss Model Based on CFD Study About the Volumetric Flow Rate Expelled by Spur Gears," *Mechanics & Industry*, vol. 13, pp. 317-323, 2012.
- [19] N. Zhao and Q. J. Jia, "Research on Windage Power Loss of Spur Gear Base on CFD," *Frontiers of Mechanical Engineering and Materials Engineering, Pts 1 and 2*, vol. 184-185, pp. 450-455, 2012.
- [20] S. Pallas, Y. Marchesse, C. Changenet, F. Ville, and P. Velex, "Application and Validation of a Simplified Numerical Approach for the Estimation of Windage Power Losses in Spur Gears," *Computers & Fluids*, vol. 84, pp. 39-45, 2013.
- [21] Y. Marchesse, N. Voeltzel, C. Changenet, F. Ville, and P. Velex, "Investigations on CFD Simulation for Predicting Windage Power Losses Generated by Helical Gears," *STLE 2014 Annual Meeting & Exhibition*, Lake Buena Vista, Florida, 2014
- [22] N. Voeltzel, Y. Marchesse, C. Changenet, F. Ville, and P. Velex, "Preliminary Numerical Investigations on Windage Power Losses Generated by Helical Gears," *International Gear Conference 2014*, pp. 1141-1149, 2014.

- [23] M. J. Hill, R. F. Kunz, R. B. Medvitz, R. F. Handschuh, L. N. Long, R. W. Noack, *et al.*, "CFD Analysis of Gear Windage Losses: Validation and Parametric Aerodynamic Studies," *Journal of Fluids Engineering*, vol. 133, p. 031103, 2011.
- [24] C. Gorla, F. Concli, K. Stahl, B.-R. Höhn, K. Michaelis, H. Schultheiß, *et al.*, "Hydraulic Losses of a Gearbox: CFD Analysis and Experiments," *Tribology International*, vol. 66, pp. 337-344, 2013.
- [25] F. Concli, C. Gorla, A. Della Torre, and G. Montenegro, "Churning Power Losses of Ordinary Gears: A New Approach Based on the Internal Fluid Dynamics Simulations," *Lubrication Science*, vol. 27, pp. 313-326, 2015.
- [26] V. T. Morgan, "The Overall Convective Heat Transfer From Smooth Circular Cylinders," *Advances in Heat Transfer*, vol. 11, pp. 199-264, 1975.
- [27] S. M. Sanchez, "Work Smarter, Not Harder: Guidelines for Designing Simulation Experiments," in *Proceedings of the 37th Conference on Winter Simulation*, pp. 69-82, 2005.
- [28] SAS Institute Inc. (10/2016). *Design of Experiments (DOE) with JMP*. Available: http://www.jmp.com/en_nl/applications/design-of-experiments.html
- [29] American Gear Manufacturers Association "AGMA 6011-I03 Specification for High Speed Helical Gear Units," ed. American Gear Manufacturers Association, p. 44, 2005.
- [30] D. W. Dudley and D. P. Townsend, *Dudley's Gear Handbook*. New York: McGraw-Hill Education, 1991.
- [31] A. A. Lord, "Experimental Investigation of Geometric and Oil Flow Effects on Gear Windage and Meshing Losses," University of Wales Swansea, 1998.
- [32] Y. Diab, "Analyse des pertes de puissance dans les transmissions par engrenages à grande vitesse: applications aux réducteurs industriels et aux machines textiles," Villeurbanne, INSA, 2005.
- [33] J. P. Kleijnen, *Design and Analysis of Simulation Experiments* vol. 20. New York: Springer, 2008.
- [34] T. El-Taweel, "Modelling and Analysis of Hybrid Electrochemical Turning-magnetic Abrasive Finishing of 6061 Al/Al₂O₃ Composite," *The International Journal of Advanced Manufacturing Technology*, vol. 37, pp. 705-714, 2008.

- [35] J. P. Kleijnen, "An Overview of the Design and Analysis of Simulation Experiments for Sensitivity Analysis," *European Journal of Operational Research*, vol. 164, pp. 287-300, 2005.
- [36] SAS Insitute Inc. (10/2016). *Creating a Response Surface Design*. Available: http://www.jmp.com/support/help/Creating_a_Response_Surface_Design.shtml

APPENDIX A

TUTORIAL FOR TWO MESHING GEAR SIMULATION IN FLUENT

The following tutorial demonstrates how to do the following:

- Set up a problem using the 2.5D dynamic re-meshing model.
- Specify dynamic mesh modeling parameters.
- Specify a rigid body motion zone and a deforming zone.
- Use prescribed motion UDF macro.
- Post process in CFD-Post.

A.1.1 Geometry and mesh

Symmetry boundary condition is imposed on mid-plane of the gearbox so that only half of the geometry needs to be modeled. Only the mesh close to the area of gear engagement will be moving as dynamic mesh. Mesh in other areas remains stationary.

Gears are separated from actual meshing so that mesh continuity is ensured, the actual central distance is therefore 95mm, instead of 92mm. The mesh is subdivided into two partitions and then imported to Fluent.

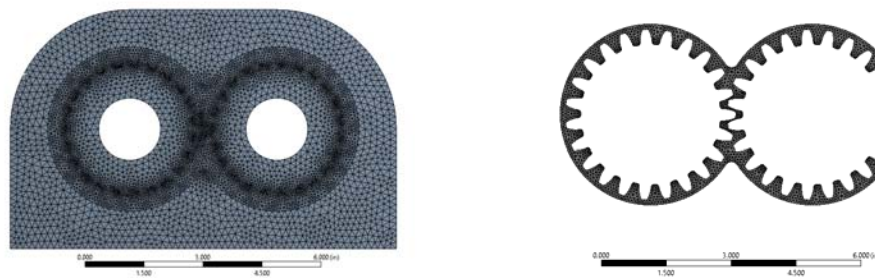


Figure A.1 Two Parts of Gearbox Mesh

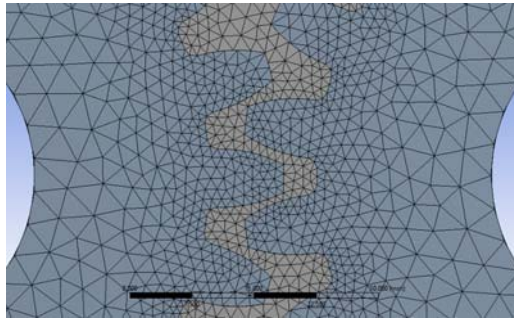


Figure A.2 Separation of Gear Teeth

A.1.2 Setup details

1) General settings

Enable 3D transient solver.

2) Models

Viscous: Realizable k-e with standard wall functions

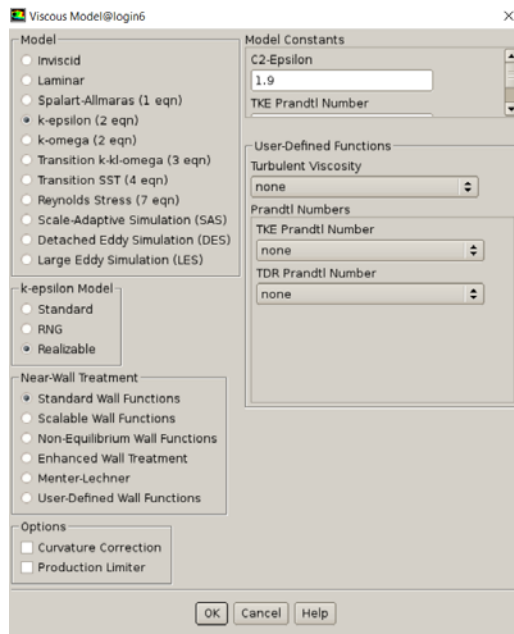


Figure A.3 Viscous Model in Fluent

3) Materials

Oil with a density of $824.5 \text{ kg} / \text{m}^3$ and viscosity of $0.005463 \text{ kg} / \text{m} \cdot \text{s}$.

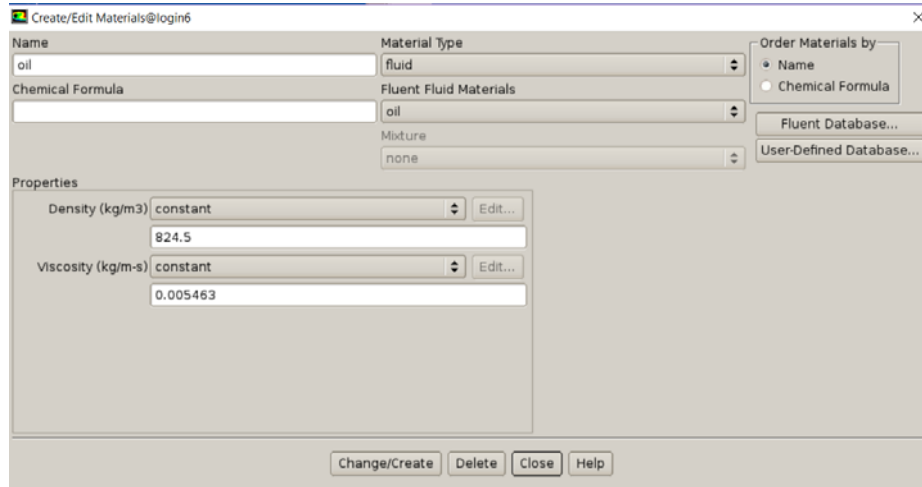


Figure A.4 Material Panel in Fluent

4) Cell zone conditions

Pick each cell zone listed and click Create/Edit. In the pop up window, make sure each cell zone is of Type Fluid and that the material selected is oil.

5) Boundary conditions

i) Mesh interface

The interface is the region which connects the two partitions. A fluid-fluid interface is defined and information at both sides can be shared through interface. The area of the interface is highlighted below.

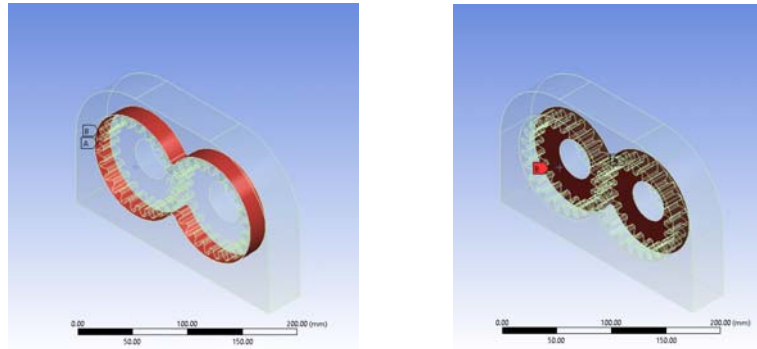


Figure A.5 Mesh Interface

ii) Symmetry boundary condition

Symmetry boundary condition (highlighted) is imposed and computational time is reduced.

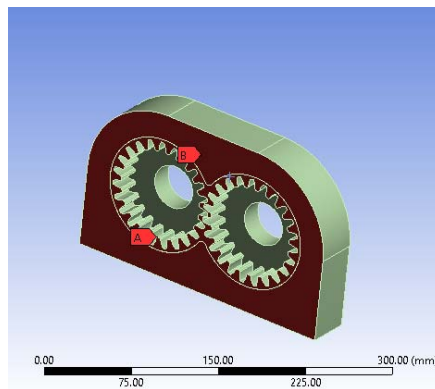


Figure A.6 Symmetry Boundary

6) Compile the UDF

The gears are set to rotate in opposite directions at a speed of 2000 rpm (209.44 rad/s). The DEFINE_CG_MOTION macro is used to define the rotation on each gear. The following UDF file is written:

```
#include "udf.h"
DEFINE_CG_MOTION(wall_gear2, dt, vel, omega, time, dtime)
{Domain *domain;
```

```

domain = Get_Domain(1);
omega[2]=209.44;}
DEFINE_CG_MOTION(wall_gear1, dt, vel, omega, time, dtime)
{Domain *domain;
domain = Get_Domain(1);
omega[2]=-209.44;}

```

7) Mesh motion setup

i) Enable dynamic mesh motion and specify the associated parameters.

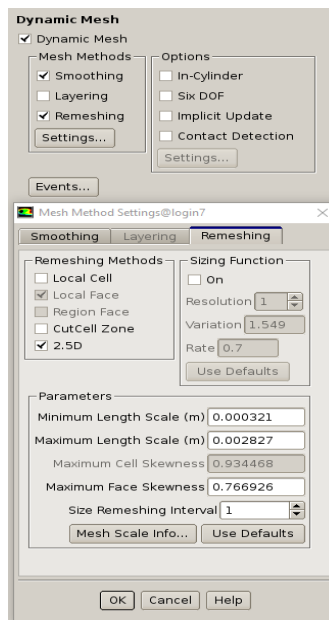


Figure A.7 Dynamic Mesh Settings

- a. Problem Setup -> Dynamic Mesh
- b. Enable Dynamic Mesh in the Models group box.
- c. Enable Smooth and Remeshing in the Mesh Methods group box.
- d. In the Mesh Method Settings panel and turn on the 2.5D remeshing method in the Remeshing tab.
- e. Click on User Defaults to set the minimum and maximum length scales.

f. Set Size Remeshing Interval to 1.

ii) Specify the motion of the wall_gear1

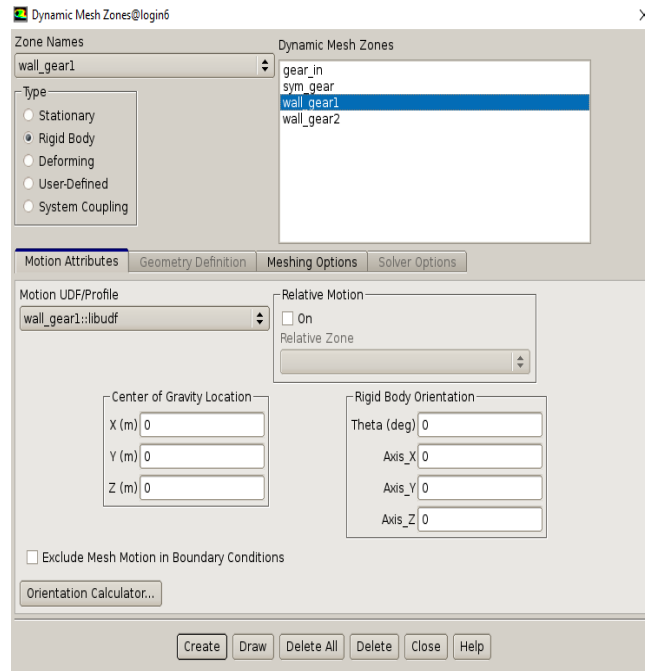


Figure A.8 Dynamic Motion Zone (Rigid Body)

- Click on Create/Edit in the Dynamic Mesh Panel.
- Select wall_gear1 from the Zone Names drop-down list.
- Retain the selection of Rigid Body in the Type list.
- Select wall_gear1::libudf from the Motion UDF/Profile
- Enter Center of Gravity location of the gear as $(X, Y, Z) = (0, 0, 0)$
- Click Create.
- FLUENT will create the dynamic zone gear1 which will be available in the Dynamic Zones list.

iii) Do the same for wall_gear2 with wall_gear2::libudf hooked to the Motion UDF panel and (0.095, 0, 0) as center of gravity.

iv) Specify the motion of the sym_gear

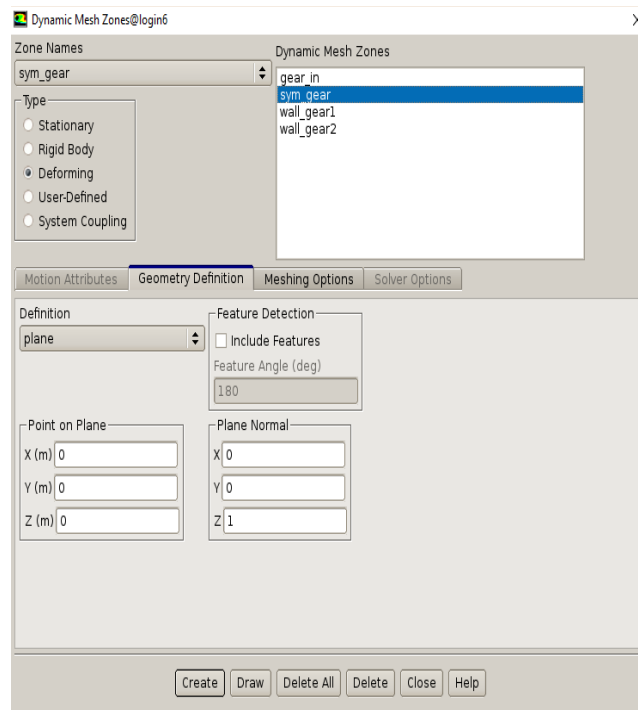


Figure A.9 Dynamic Mesh Zone (Deforming_Geometry Definition)

- Select sym_gear from the Zone Names drop-down list.
- Select Deforming from the Type list.
- In the Geometry definition tab, turn Definition to plane, specify point on the plane as (0,0,0) m and the plane normal as (0,0,1). This ensures that re-meshing does not cause the mesh to move out of the specified plane.

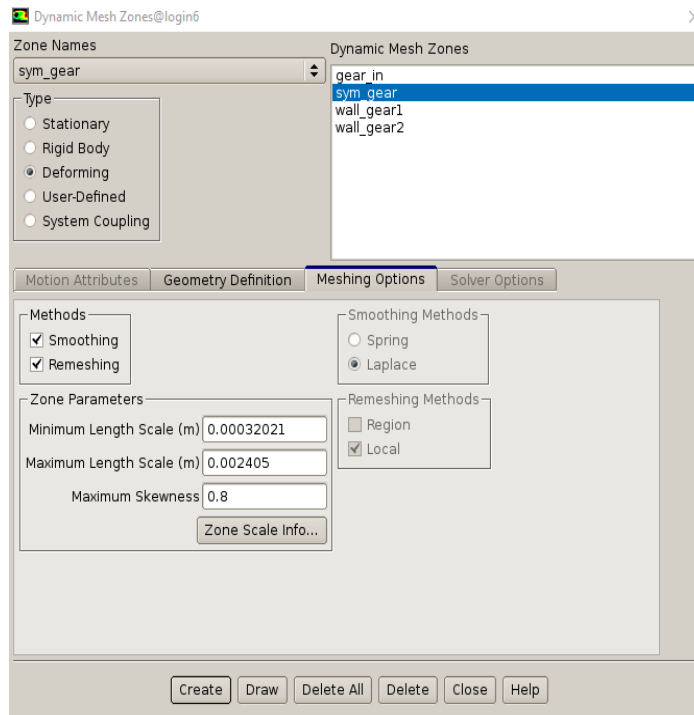


Figure A.10 Dynamic Mesh Zone (Deforming_mesh Options)

- d. Click the Meshing Options tab and set the following parameters:
- e. Enable Smoothing and Remeshing in the Methods group box.
- f. Specify Minimum and Maximum length scales as 0.0003 and 0.002 respectively. The "Zone Scale Info" button gives information on the minimum and maximum length scales in the domain and can be used as a guide to set the above values.
- g. The Maximum skewness is set to 0.8.
- h. Click Create.

FLUENT will create the dynamic zone `sym_gear` which will be available in the Dynamic zones list.

- iv) Do the same for `gear_in`

a. For the zone, in the Meshing Options tab be sure to turn off Remeshing and enable only Smoothing.

b. In Geometry Definition tab, the point on the plane is (0,0,-0.02) with plane normal (0,0,1).

vi) Displaying the Zone Motion

a. Click on Display Zone Motion button in the Dynamic Mesh Panel

b. Enter time step size to be 5e-6

c. Number of steps is 100

d. Preview

e. This shows the rotation of the zone as a preview. This helps to make sure that the UDF is specifying the motion of the zone correctly.

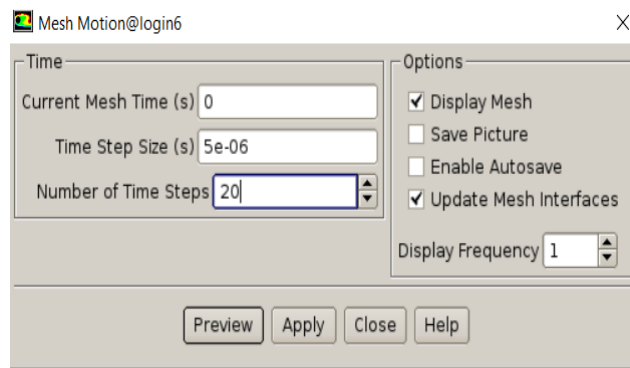


Figure A.11 Previewing the mesh motion

viii) Similarly, the mesh motion can be displayed

a. Click on Preview Mesh Motion

b. Display the mesh on the geometry by going to Graphics and Anomations -> Mesh-> Setup

c. Enter time step size to be 5e-6

d. Number of time steps 20

e. Preview

f. This shows the gears motion and remeshing for the specified number of time steps.

8) Solution

i) Request saving of case and data file every 100 time steps.

a. Solution -> Calculation Activities -> Autosave

b. Enter 500 after Autosave Every (Time Steps). Clicking on Edit makes more options available.

ii) Write out CFD-Post compatible files for transient data post processing in the interests of minimizing hard disk space

a. Calculation Activities > Automatic Export > Create > Solution Data Export.

b. Choose file type to be CFD-Post compatible.

c. Select Frequency to be 20

d. Select (Static Pressure, Velocity Magnitude, X Velocity, Y Velocity, Z Velocity, X-Coordinate, Y-Coordinate, Z-Coordinate and Density as variables to post process)

iii) Solution methods

Change pressure discretization to "PRESTO!". Retain the rest of the choice.

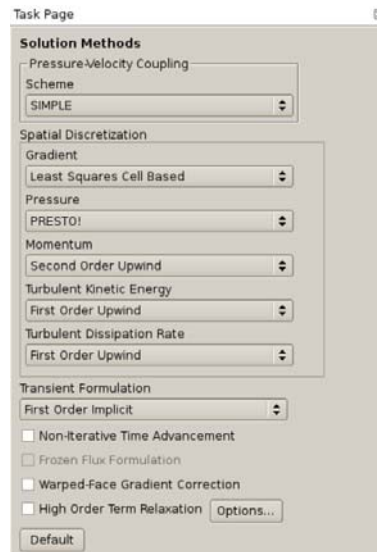


Figure A.12 Solution methods

iv) Solution Controls

Retain defaults.

v) Initialize the flow field

- a. Solution-> Solution Initialization -> Initialize
- b. Set Gauge Pressure to be 101325 Pa.

vii) Run the calculation for 5000 time steps

- a. Solution -> Run Calculation
- b. Enter $5e-6$ s for Time Step Size.
- c. Enter 5000 for Number of Time Steps.
- d. Set Max Iterations/Time Step to 20.
- e. Click Calculate

APPENDIX B

TUTORIAL FOR COUPLING GUARD TEMPERATURE SIMULATION IN CFX

To further instruct readers to carry out CFD simulation of coupling guard temperature, a step by step tutorial is written. The tutorial demonstrates how to do the following:

- Geometry import and mesh generation in ANSYS Workbench
- Boundary conditions setup
- Input of heat transfer coefficient in CFX
- Post-processing in CFD-POST

B.1 Geometry and meshing

The geometry of the baseline model is built in SolidWorks, dimensions are listed below:

Table B.1 Gear Geometry for Sample Case

No	DBFF (inch)	Rotating Speed (rpm)	Max Diameter (inch)	Radial Clearance (inch)	Shaft Temperature (°F)	Ambient Temperature (°F)	No. of Bolts
Sample 1	25	3600	24	2	120	100	36

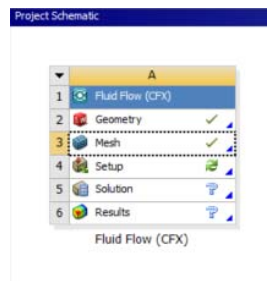


Figure A.13 Fluid Flow Analysis in ANSYS Workbench

The geometry is imported to ANSYS Workbench, where mesh is generated.

- 1) Click setup and choose Edit.

B.2 Setup details

In CFX, computational domain is divided into 3 parts:

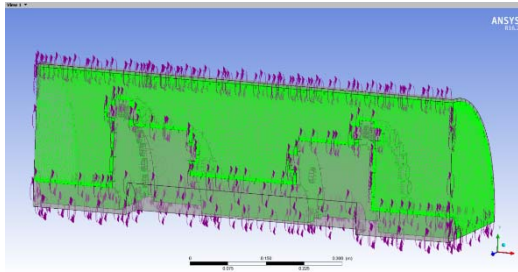


Figure A.14 Outerfluid Domain (Fluid)

1) Outerfluid Domain

- a. Basic settings

Material = Air Ideal Gas

Angular Velocity = 3600 [rpm]

Rotation Axis = Global X

- b. Fluid Models

Heat transfer option = Total Energy (Include Viscous Work Term)

Turbulence option = Shear Stress Transport

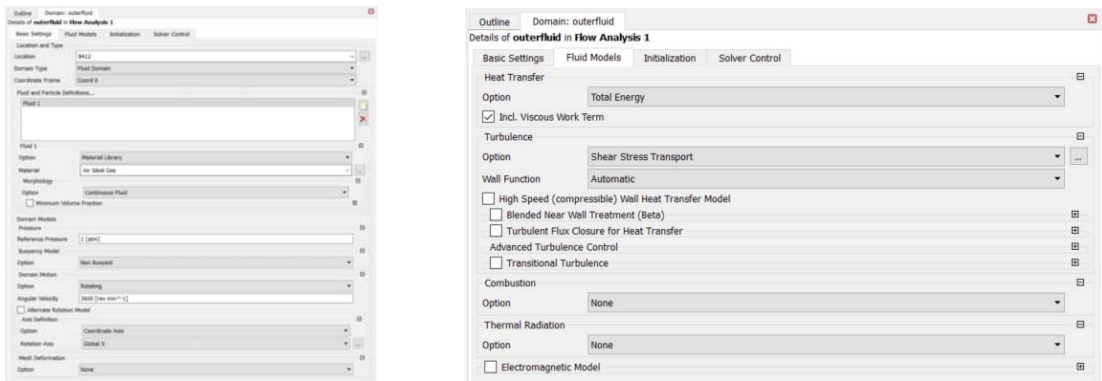


Figure A.15 Settings for Outerfluid Domain

2) Shroud Domain

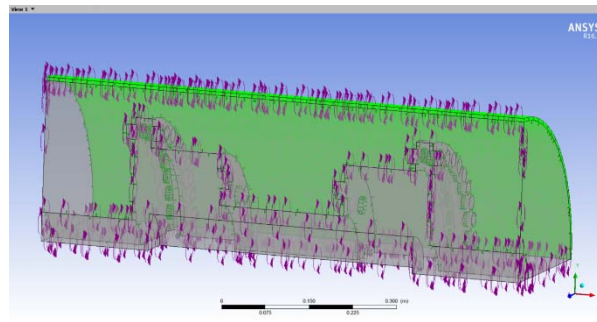


Figure A.16 Shroud domain (Solid)

- a. Basic settings
 - Material = Steel
 - Domain motion = Stationary
- b. Solid models
 - Heat transfer option = Thermal Energy

Heat transfer coefficient is imposed on outer surface of shroud, with ambient temperature 100 °F. The expression for heat transfer coefficient is written in section 2 based on empirical formula.

2) Solid Domain

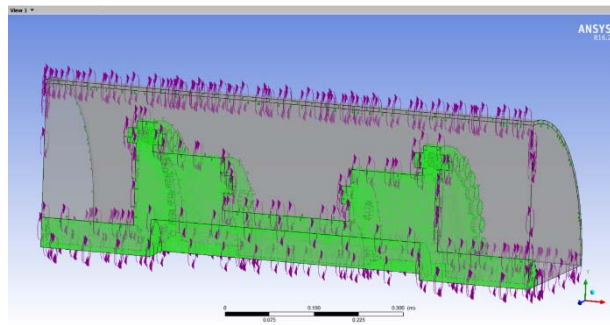


Figure A.17 Coupling domain (Solid)

a. Basic settings

Domain motion = 3600 [rpm]

Rotation Axis = Global X

b. Solid models

Heat transfer option = Thermal Energy

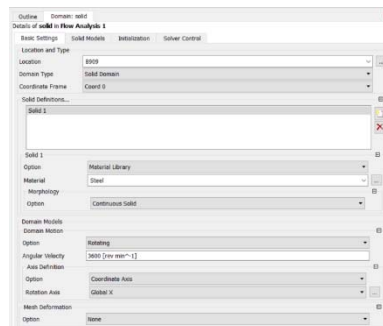


Figure A.18 Settings for Coupling Domain

a. Boundary details in Shaft_inlet

Shaft temperature = 120F

3) Interfaces

- a. outerfluid_periodic
- b. shroud_periodic
- c. solid_periodic
- d. domain Interface 1, interface between coupling outer surface and surrounding fluid
- e. shroud_outerfluid, interface between inner surface of the shroud and surrounding fluid

Interface a - c are periodic boundary conditions; interface model option is Rotational Periodicity with Global X axis.

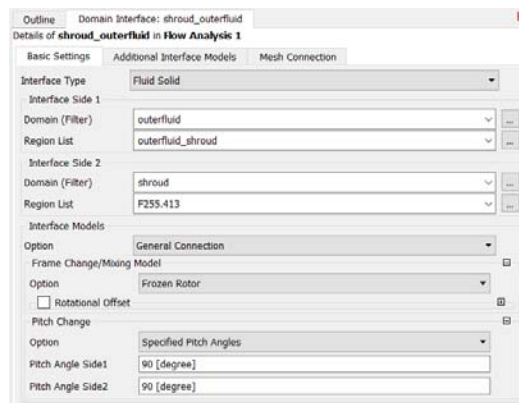


Figure A.19 Settings for Shroud_outerfluid interface

Interface d-e are General Connection. For interface e, frame change/ mixing model is Frozen Rotor, specified Pitch angles with pitch angle at both sides = 90 [degree]

The outline after all the boundary conditions have been entered:

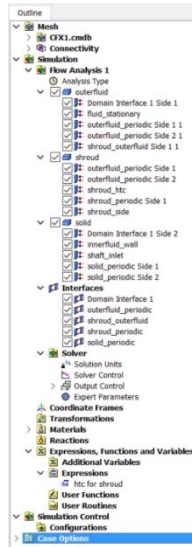


Figure A.20 Outline of Boundary Conditions in CFX

APPENDIX C

DESIGN OF EXPERIMENTS IN JMP

Traditionally, in order to study the effect of several factors on one response, only one factor is changed at a time. The main disadvantage of this practice is that it does not include interactive effect of the factors on the response. While full factorial design covers all possible combination of a set of factors, it is not practical in most applications due to the large sample size.

Design of Experiment (DOE) is a scientific way to find factors set and minimize simulation runs. Response Surface Methodology (RSM) consists of a group of mathematical and statistical techniques and used in the response surface design to find the optimal response within specified ranges of the factors. The most popular response surface design is the central composite design.

DOE function in JMP helps to reveal the joint effect of factors on response. Instead of changing one parameter at a time, multifactor experiments are designed. DOE minimizes simulation cost while test out both individual effect and combined effect of two or more factors.

During the development of regression model in section 2 & 4, input parameters are identified and range for each parameter is assigned. In JMP, both Custom Design and Response Surface Design options within DOE are used. It provides minimum number of simulation runs that can estimate the required effect of input on response. A second-order prediction formula for the response can be fitted by these designs. [36]

Below is an example describing DOE process in section 4. Factors and response is entered and Central Composite Design is chosen as design type.

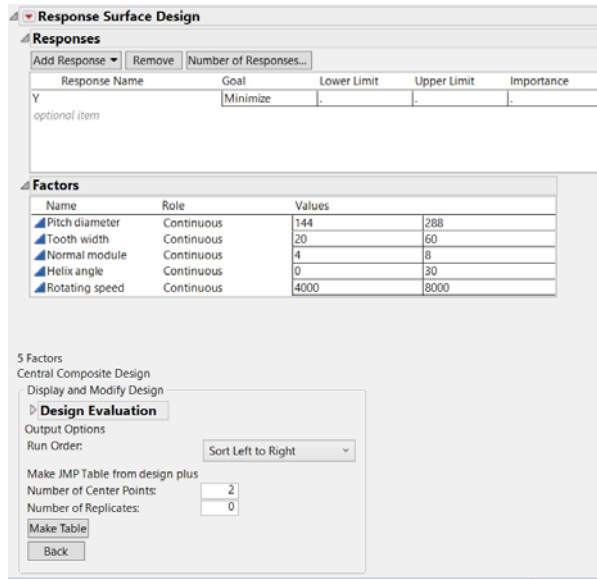


Figure A.21 Response Surface Design in JMP

Click Make Table, a simulation experiment design with 28 simulation runs is generated. Note that response Y is to be determined by simulation results from ANSYS CFX.

	Pattern	Pitch diameter	Tooth width	Normal module	Helix angle	Rotating speed	Y
1	-----	144	20	4	0	4000	•
2	---+--	144	20	4	30	8000	•
3	--++--	144	20	8	0	8000	•
4	-++--	144	20	8	30	4000	•
5	a0000	144	40	6	15	6000	•
6	-++--	144	60	4	0	8000	•
7	-++--	144	60	4	30	4000	•
8	-++--	144	60	8	0	4000	•
9	-++++	144	60	8	30	8000	•
10	0a000	216	20	6	15	6000	•
11	00a00	216	40	4	15	6000	•
12	000a0	216	40	6	0	6000	•
13	0000a	216	40	6	15	4000	•
14	00000	216	40	6	15	6000	•
15	00000	216	40	6	15	6000	•
16	0000A	216	40	6	15	8000	•
17	000A0	216	40	6	30	6000	•
18	00A00	216	40	8	15	6000	•
19	0A000	216	60	6	15	6000	•
20	+----+	288	20	4	0	8000	•
21	+--+-	288	20	4	30	4000	•
22	+--+--	288	20	8	0	4000	•
23	+----+	288	20	8	30	8000	•
24	A0000	288	40	6	15	6000	•
25	+----	288	60	4	0	4000	•
26	+----	288	60	4	30	8000	•
27	+----	288	60	8	0	8000	•
28	+----	288	60	8	30	4000	•

Figure A.22 DOE Results in JMP

After all the response values (Y) are obtained from CFD-POST, they are entered in the Y column. A prediction formula is generated using Fit Model and the formula is rewritten in MATLAB.